CHALMERS
UNIVERSITY OF TECHNOLOGY

The Effect of Ion Interactions on the Photoactivity of Pentacene- and Anthracene Carboxylic Acid

Can ion-ion bridges facilitate singlet fission?

Master's thesis in Material Chemistry

HANNA LARSSON

DEPARTMENT OF CHEMISTRY AND CHEMICAL ENGINEERING

CHALMERS UNIVERSITY OF TECHNOLOGY

Gothenburg, Sweden 2023
www.chalmers.se

The Effect of Ion Interactions on the Photoactivity of Pentacene- and Anthracene Carboxylic Acid

Can ion-ion bridges facilitate singlet fission?

HANNA LARSSON

CHALMERS
UNIVERSITY OF TECHNOLOGY

Department of Chemistry and Chemical Engineering

Division of Chemistry and Biochemistry

Maria Abrahamsson´s research group

CHALMERS UNIVERSITY of TECHNOLOGY

Gothenburg, Sweden 2023

The Effect of Ion Interactions on the Photoactivity of Pentacene- and Anthracene Carboxylic Acid

Can ion-ion bridges facilitate singlet fission?

HANNA LARSSON

Supervisors: Andrew Brian Maurer, Division of Chemistry and Biochemistry, Chalmers University of Technology,

Maria Abrahamson, Division of Chemistry and Biochemistry, Chalmers University of Technology

Examiner: Maria Abrahamson, Division of Chemistry and Biochemistry, Chalmers University of Technology

Master's Thesis 2023

Department of Chemistry and Chemical engineering

Chalmers University of Technology

SE-412 96 Gothenburg

Telephone +46 31 772 1000

The Effect of Ion Interactions on the Photoactivity of Pentacene- and Anthracene Carboxylic Acid
Can ion-ion bridges facilitate singlet fission?

HANNA LARSSON
Department of Chemistry and Chemical Engineering
Chalmers University of Technology

Abstract

Efficiency of solar panels can be improved by incorporating up- and downconverting materials, improving the utilization of the sun irradiation and thus amplify the photocurrent. Within this thesis the downconverting process, singlet fission, where a singlet excited state can be converted to two triplet states that are lower in energy is of interest. However, the mechanisms behind it are yet not fully understood and thus it is troublesome to design and find efficient systems. Moreover, singlet fission works only at high concentration or by cleaver design, e.g., by covalently bind the chromophores together. Therefore, a new approach where ion-ion coupling between the chromophores has been investigated. Aiming to further understand the processes and finding a system operating at low concentration.

The photochemistry of the chromophores 9-anthracene carboxylic acid (ACA) and 4-(6,13-bis((triisopropylsilyl)ethynyl)pentacene-2-yl)benzoic acid (PCA) have been studied and how it is affected by deprotonation and interaction with metal-sulphate salts. Deprotonation has been proven to quench the emission and lower the emission lifetime. For ACA, deprotonation leads to a redshift in absorption and a blueshift in emission, addition of $MgSO_4$ and $ZnSO_4$ results in a partial deprotonation and stabilization of the negative charge on deprotonated ACA. The addition of base to PCA has less effect on its photochemistry, however the emission is still quenched, and the absorption is slightly broadened. Formation of chromophore complexes has been indicated. The emission lifetime and transient absorption have been studied and have shown to be affected by ion-ion interactions and deprotonation of the chromophore. Singlet fission has not been detected within the systems yet, however more measurements are still needed to say anything with accuracy.

Keywords: Ion-ion interactions, singlet fission, 9-anthracene carboxylic acid, TIPS-pentacene carboxylic acid,

Acknowledgment

I would like to give a big thanks to my supervisors Andrew Brian Maurer and Maria Abrahamson, who guided me throughout the project. You have let me be independent and test my ideas, simultaneously as I felt cared for, and supported. You have challenged and led me to become a better problem solver, and for that I'm truly grateful.

Andrew, I think that we both share a love for science, thank you for always being there for me. From practical issues to theoretical discussions, I have learned so much about photochemistry just from listening to you. If only a smudge of your knowledge has rubbed off on me, I would be happy.

Maria, thanks for letting me perform my master's thesis project within your group. Thank you for letting curiosity be the driving force in the project, allowing me to follow my interest, and supervising me along the way. You always have suggestions of solutions and answers to my and others' problems, building a firm foundation in the group and great support. Your leadership and knowledge are inspiring.

I want to take the moment to thank the rest of the group. Axel, Deise, Fredrik, Hassan, Liam, Rasmus, Wera, and Wilma, thank you for all the encouragement, help, and support that you all have given me during the project. You have inspired me to become a better researcher, giving me hope when experiments failed, and practical help when needed. Especially thanks to Liam for the help with the ITC experiments and analysis, Hassan for the help with NMR and finding chemicals, and Rasmus for the help with femtosecond measurements.

Moreover, thanks to all my office mates, you made this experience so much more enjoyable, and I wish you all the best. Lastly, thanks to my friends and family, for being genuinely supportive and cheering me along the way.

Hanna Larsson, Gothenburg, January 2023

Table of contents

1. Introduction

The ongoing climate crisis is not something we can look away from, each year new reports about the situation, and the standing conclusion is that we need to make large efforts to change towards a more sustainable world. On top of that, we are also facing a falling economy, an energy crisis, and considerable social challenges. Nevertheless, the work toward a more sustainable future can be seen in large parts of society and academia. Projects that aim to find new materials, focus on energy supply and distribution, or increase recyclability, are just a few examples.

Solar energy is an important part of the transition toward a more sustainable society. To solve the energy crisis, which is more relevant now than ever, efficient solar cells are key. In 2021 the global installation of solar energy reached a record of 133 GW, representing almost 40 % of the total power addition worldwide. Still, the integration of renewable energy needs to increase continuously if the goal of 1.5 ˚C global heating should not be exceeded [1]. The efficiency of solar panels has in the last decades increased greatly, and the best crystalline silicon cells, which are the most common type, have efficiencies in the interval of 21.2-27.6 % [2]. The theoretical upper limit for a single p-n junction cell is 33 %, called the Shockley-Queisser limit, for a silicon cell it is down to 30 % based on the irradiation and the silicon bandgap on 1.1 eV [3]. To surpass the theoretical maximum different approaches could be applied. Nozik et al. proposed in 2006 the possibility to increasing the efficiency of solar cells by incorporating singlet fission (SF) material into a single-junction cell [4]. A SF material utilizes the excess energy that high-energy photons have and down-converts them to photons with lower energy, simultaneously increasing the number of photons [5]. Hence, a higher photocurrent in a photovoltaic (PV) can be produced by converting high-energy photons to multiple excitation states [6, 7]. Since 2006, the interest in SF material has increased avalanche-like, thus the total efficiency of the solar cell is predicted to reach 45 % from the previously mentioned 33 % [8]. SF is an example of multiple excitation generation (MEG); materials with these properties are considered one of the most promising processes to break the theoretical limit [9]. However, there are still some theoretical and practical obstacles before it will be fully implanted on a large scale.

Some of the most researched SF systems are acenes such as pentacene and tetracene. They have been used to understand the underlying mechanisms of SF, which is still to this day somewhat debated. When SF materials have been added to solar panels, the efficiency increases [10, 11]. SF has been observed in crystals, films, and solutions. One problem to overcome is to avoid the opposite process of recombination, also known as triplet-triplet annihilation (TTA) [6]. The thickness of the SF material is also of importance, it must absorb photons with high energy and let others reach the other layers underneath. The photons/ charge carriers generated must reach the silicon layer in the cell to be converted to electricity [12]. A system that could operate at low concentrations is therefore preferable.

SF can occur at discernibly lower concentrations by chemically bind the chromophores together compared to free monomers in solution. There are several examples where different approaches have been used to confine the orientation of the chromophore to increase the formation of multiple excitation states (MES). Incorporated into films, adsorbed on quantum dots, different covalent bridges where the length, conjugation, and position have been studied [5, 13-15]. Nevertheless, covalent bonds increase the probability of TTA. In this work, ion-ion interactions are instead investigated. The hypothesis is that if chromophores can form complexes with a cation, a conformation with desirable orientation and distance of the chromophores can be

achieved. Moreover, if the dissociation rate, k_{off}, between the chromophores and the ion is slower than the triplet formation through SF, $k_{triplet}$, and/or faster than the TTA rate, k_{TTA}, an efficient SF-system would potentially be reached. The suggested progression will be more deeply described in Section 2.2.

A prerequisite for forming ion-ion bonds between a cation and a chromophore is forming a negative charge on the chromophore. This study investigates if ion-ion bonds could be achieved by deprotonating carboxylic acids on acenes and then combine them with cations. 4-(6,13-bis((triisopropylsilyl)ethynyl) pentacene-2-yl) benzoic acid (PCA) was synthesized before the study, see Figure 1 for chemical structure. As previously mentioned pentacene is known to be able to undergo SF. However, due to PCAs' low stability and its inherent complicated photochemistry, a model system with 9-anthracene carboxylic acid (ACA) with simpler structure and analysis was initially used, see Figure 1 for chemical structure.

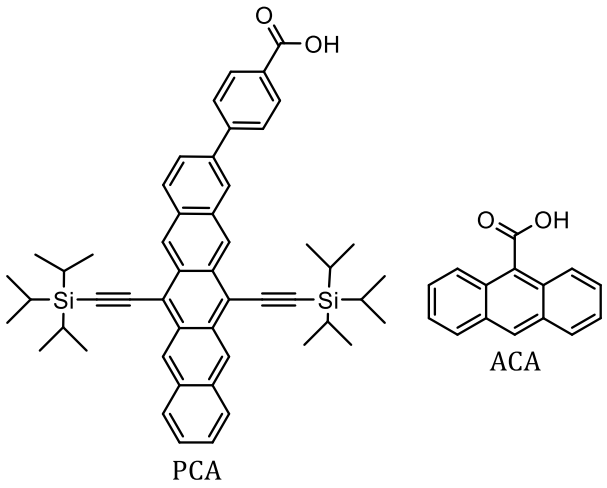

Figure 1 *Chemical structure of (from left to right) 4-(6,13-bis((triisopropylsilyl)ethynyl)pentacene-2-yl)benzoic acid (PCA) and anthracene 9-carboxylic acid (ACA).*

Deprotonation of the carboxylic acids was achieved using two different bases, one ionic (tetrabutylammonium hydroxide, TBAOH) and one organic (diazabicycloundecene, DBU). Investigations of ion-ion interactions, multiple cations were tested, all with sulphate as a counterion to abridge the analysis. The effect on the photochemistry was studied by were steady-state absorption, emission, and excitation, time correlated single photon counting (TCSPC), transient absorption (TA), and isothermal titration calorimetry (ITC). After conducting these experiments with ACA, the best conditions were applied to PCA. An overview of type of experiments conducted is present in Supporting information S.1.

This work is an extension to a previously conducted 15-credit project. Some of the results obtained under its duration will be presented within this thesis to give a more holistic description and a better foundation of the results. All work with PCA, all combinations of salts except $ZnSO_4$, all transient absorption, and isothermal titration calorimetry measurements are novel to this work.

1.1 Questions of interest

The main aim of the project is to investigate if SF can be facilitated by connecting chromophores together with week ion-ion bridges with a cation as a link between them, the hypothesis will be further discussed in Section 2.2, and the mechanism illustrated in Figure 4. To be able to answer

that question, several sub-subjects need to be addressed prior and will be the focus of this thesis. How is the photochemistry affected by deprotonation? Can chromophore-ion complexes be formed? Which prerequisites are needed to be fulfilled? If complexes are formed, how is the photochemistry of the chromophores affected?

1.2 Objective and aim

The objective of the project is to form a foundation of understanding and knowledge about the chemical and photoactive principles of ACA and PCA so that the possibility to undergo SF can be investigated further. In the future, if SF can be shown for a system like this, information about the underlying mechanisms could be extracted. Hence, the size and type of cation can be changed, a disarticulation between energy or electron transfer could possibly be done, and the position of chromophores relative to each other can be deeper investigated. Subsequently, better SF systems can be created.

The scope of this project will not include the characterization of SF mechanisms, instead focus will be on the formation of chromophore complexes. Aiming to find conditions that later can be used when investigating the SF mechanisms.

1.3 Limitations

To observe how ion-ion interaction affects the chromophore of interest, the project was divided into two parts. One part where a model system with ACA, a chromophore with higher stability, easier analysis, and that is commercially available, was studied. Obtaining knowledge about deprotonation, solubility, and ion-ion interactions. In the second part the insights were applied to a system with PCA where SF is a possible process to occur. However, the translation between the two molecules is not straightforward, there are differences between the two systems resulting in different solubility, photochemical properties, and reactivity. Hence, the knowledge gathered from the model system cannot be directly used for the PCA system.

Moreover, the PCA itself is also a model system in the sense that it would become difficult to incorporate it onto solar panels due to its low chemical and light stability. Pentacene is widely researched to understand the mechanisms of SF, but its light sensitivity needs to be dealt with if a commercial product would be created with it as a down conversion material. The connection to a real and practical device is outside of the scope of this project. Another factor that needs to be considered is solubility, the chromophores are nonpolar, and by charging them through deprotonation the solubility could be largely affected. The solubility is not investigated further.

2. Theory

The following part provides fundamental theory about the subject to assist in interpreting the following results and discussion. Firstly, a brief background of spectroscopy and some selected key points will be highlighted. The phenomena singlet fission and the proposed progression will thereafter be presented, and the most important factors of designing a SF system will be introduced. Secondly, an overview of solar energy and solar panels will be given, which limitation they have and different strategies in overcoming them. Thirdly, theory behind ion-ion interactions and deprotonation will be established, followed by an introduction of the techniques mostly used within the project.

2.1 Light and matter interactions

First, to understand how our society better can utilize the energy from the sun, some knowledge about how light and matter interact with each other is needed. All information in the following section is gathered from the book Modern Spectroscopy 4th edition by J. Michael Hollas [16] if not stated otherwise. Spectroscopy is the scientific area where the interaction between light and matter is studied. Radiation energy can be seen as an electromagnetic wave with a wavelength, λ, or as a particle, a photon with a specific energy. Light can interact with matter by being absorbed, scattered, or reflected. The energy, E, that a photon carry is related by the Planck constant, h, and the speed of light, c, the frequency, ν, and wavelength, see Equation 1.

$$\Delta E = \frac{hc}{\lambda} = h\nu \tag{1}$$

Hence, the radiation energy is quantized, meaning that one can see the energy as quanta with a specific amount of energy carried. Several different units can be useful when working with spectroscopy e.g., wavelength [nm], wavenumber [cm^{-1}], Joule [J], or electronvolts [eV].

Atoms and molecules have specific energy levels, called atomic orbitals, AO, and molecular orbitals, MO. The MO can be derived by a linear combination of the AO. Moreover, there are vibrational and rotational modes that also have specific energy levels coupled to them. Only certain transitions are possible, in other words, the added energy must match the energy levels for a molecule to be excited. The molecule can be exited rotationally, vibrationally, or electronically dependent on how much energy is absorbed. Simultaneous transitions are possible, e.g., vibronic transitions are those when the molecule goes through both electronic and vibrational transitions in one step. Additionally, specific selection rules for the transitions can be derived that determine which shifts to which states are allowed, and which have a higher probability of occurring. At equilibrium, the Boltzmann distribution law is valid, see Equation 2, generating the relation of energy, ΔE, temperature, T, and the population (N) at energy state n and m, N_n and N_m, k is the Boltzmann constant.

$$\frac{N_n}{N_m} = \exp\left(-\frac{\Delta E}{kT}\right) \tag{2}$$

If energy is absorbed, the molecule gets excited and undergoes a transition to a higher energy level. Electronically excited states can be divided depending on the spin quantum number and configuration of electrons of individual states singlets such as, S_n, triplets, T_n, or quintets, Q_n. Singlets have a total spin number S=0, triplets have two unpaired electrons, and a quantum spin number equal to 1. After excitation, the system will eventually decay back to the ground state, provided that the system has no photoreactivity. There are multiple decay paths, emission of a photon, called luminescence, or through nonradiative decay, for example, vibrational relaxation.

The system can also undergo internal conversion (IC) or inter-system crossing (ISC), going from one state to another. All these processes are present simultaneously, to various extents for different systems, and are often competing. Emission from a singlet state is called fluorescence and emission from a triplet state is called phosphorescence.

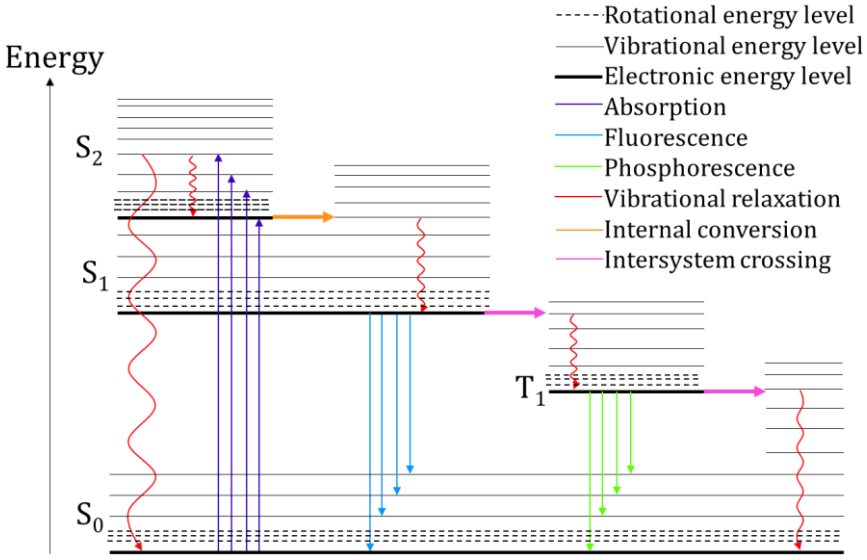

Figure 2 *Jablonski type diagram that shows an excitation from the ground state, S_0, to the second electronically excited state, S_2, and the different possible decay pathways, vibrational relaxation, fluorescence, and phosphorescence. Moreover, transitions between electronically excited states, internal conversion (IC), and intersystem crossing (ISC) are included. Some vibrational and rotational levels are displayed, keep in mind that there are rotational modes between every vibrational level, these were excluded to ease the figure interpretation. Excitation can also occur to the lowest excited singlet state S_1. T_1 denotes the lowest triplet excited state which can be reached through spin-forbidden transitions.*

In Figure 2 a Jablonski type diagram is presented where different transitions possible in a system are displayed. Emission is shown as a transition from the lowest vibrational level of S_1 to the ground state, following Kasha's rule. It states that emission originates from the lowest level in the excited multiplicity [17]. Moreover, it results in that the fluorescence is generally independent of excitation wavelength. In 1852 discovered Sir G. G. Stokes. that the emitted light had less energy than the probing light. Hence there is a shift between the absorption and the emission spectra, called the Stokes shift. It is commonly caused by the rapid decay to the lowest vibrational level of S_1. Although emission in some cases can occur from higher electronic excited states it is quite unusual. A small Stokes shift can results in reabsorption, also known as inner filter effects [18].

During excitation, the transitions where the electrons keep their spin are allowed, and spin flips are forbidden transitions. Hence, if the ground state is a singlet, the excited state is normally a singlet, thus, no spin-flip is needed. However, triplets can be formed through forbidden transitions, often a singlet is first formed, and then through ISC triplets can be formed. The lifetime of the excited state is also dependent on the spin of the electrons, thus if a spin-flip is necessary for returning to the ground state the rate is often increased. The lifetime of a singlet state is generally around 10 ns or below, and the lifetime of a triplet is generally longer, between 100 to 1000 ns [6].

The excitation of a molecule can strengthen or weaken a chemical bond if the vibrational mode frequency is changed. When a molecule is electronically excited, many vibrational modes are crossed. According to the Franck-Condon principle only vertical transitions is allowed. Hence, the vibrational mode may not be the same in the excided state as in the ground state as the potential surfaces might be positioned differently compared to each other. The rate of electronic transitions

is substantially faster than nuclei moves, after vibrational decay at the excited state, the equilibrium distance of the nuclei can change, resulting in different strengths in the chemical bond [19]. Thus, the lifetime of the excited state can be extended as the equilibrium distance in the ground state must be resumed as the emission also follows the Franck-Condon principle.

It will soon be clear why the emission lifetime is important. In SF, processes occur in the excited state of a molecule. Hence, for a system to undergo SF one wants to have as few competing processes as possible and that they are slower than the rate of SF. Moreover, triplets generally have a longer emission lifetime compared to singlets as previously mentioned, in SF two triplets are formed which results in more time for the separation of the excited states. In the following sections the mechanisms of SF will be presented more in depth.

2.2 Singlet fission

Singlet fission (SF) is a spin-allowed phenomenon in which one singlet excited state, S_1, is divided into two triplet excited states, T_1 [5, 9, 20, 21]. The first observation and conformation of SF was presented in the 1960s for tetracene and anthracene crystals [22]. Two different mechanisms can explain the process, (i) direct coupling to the triplet excited state from the singlet excited state or (ii) an intermediate charge transfer state [5]. In the direct mechanism, S_1 relaxes non-radiatively with a singlet character, named multiexciton state, to a pair of triplet excited states ^{1}(TT) [23]. While in the other process, an intermediate state is present as a charge-transfer (CT) state with higher energy before the relaxation of S_1, and therefore called a mediated mechanism, including two different steps. The CT state can be virtual or real [9]. A simplification of the direct mechanism is presented in Figure 3. The progression is still not fully understood and seems to be largely affected by the chemical environment. Hence, it is difficult to draw any universal conclusions [15, 24].

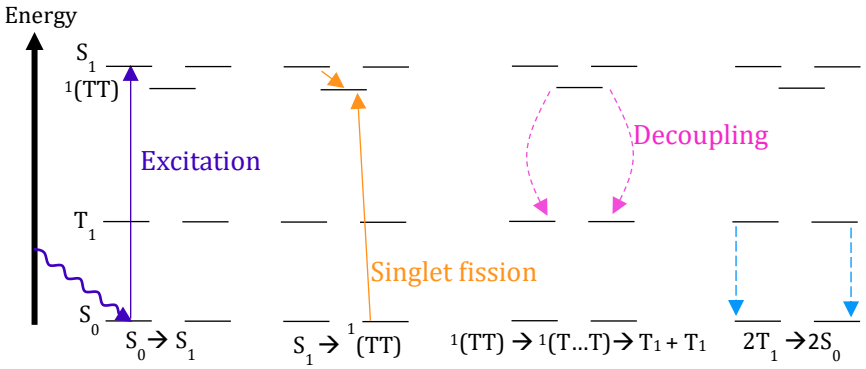

Figure 3 *Illustration of progression during SF. Initiated by the excitation of one chromophore to its singlet excited state, S_1. A triplet-triplet coupled state (^{1}(TT)) is formed as the singlet excited electron and an electron at another chromophore in ground state (S_0) undergoes SF. The ^{1}(TT)) creates a triplet-triplet decoupled pair ^{1}(T…T)) and forms thereafter two separate triplets (T_1) that can return to the ground state (S_0) through multiple decay paths. The total multiplicity is kept throughout the process, hence, spin-allowed process.*

The creation of free triplets, T_1, is preceded by the formation of a coupled triplet-triplet state, ^{1}(TT). The procedure of the direct mechanism can be written as:

$$S_0 + S_1 \rightarrow {}^1(TT) \rightarrow {}^1(T\ldots T) \rightarrow T_1 + T_1$$

where S_0 denotes the ground state of one chromophore, and S_1 is the lowest singlet excited state for another. ^{1}(TT) stands for the triplet pair when it is electronically coupled and ^{1}(T…T) when it's electronically decoupled [23]. The ^{1}(TT) is a multiexciton state, where two triplets are

electronically coupled and spin entangled. It has been shown that this state has its own non-radiative decay and symmetry-forbidden fluorescence via the Herzberg-Teller mechanism[22].

For SF to occur, three constraints must be fulfilled; (i) the energy level of S_1 must be twice or more than T_1, $E(S_1) \geq 2E(T_1)$, (ii) the rate of SF must exceed other decay pathways, such as ISC and IC, and (iii) the triplets must be separated so that the system does not undergo the opposite process of TTA. The rate of formation of the $^1(TT)$ state depends on the energy states and the electronic coupling between them [8]. Hence, energy matching is important to gain a working SF system. To decrease the rate and possibility of TTA, the energy constraint $E(T_2) \geq 2E(T_1)$ should be fulfilled.

Moreover, the chromophore must absorb strongly, and the triplet energy match the bandgap of the solar panel to be a viable candidate to increase the photocurrent by SF. The lifetime of the triplet excited state must exceed the separation rate to form two electron-hole pairs. Additionally, the coupling of the chromophores influences the SF process [9]. In other words, finding a system SF system that works can be quite intricate.

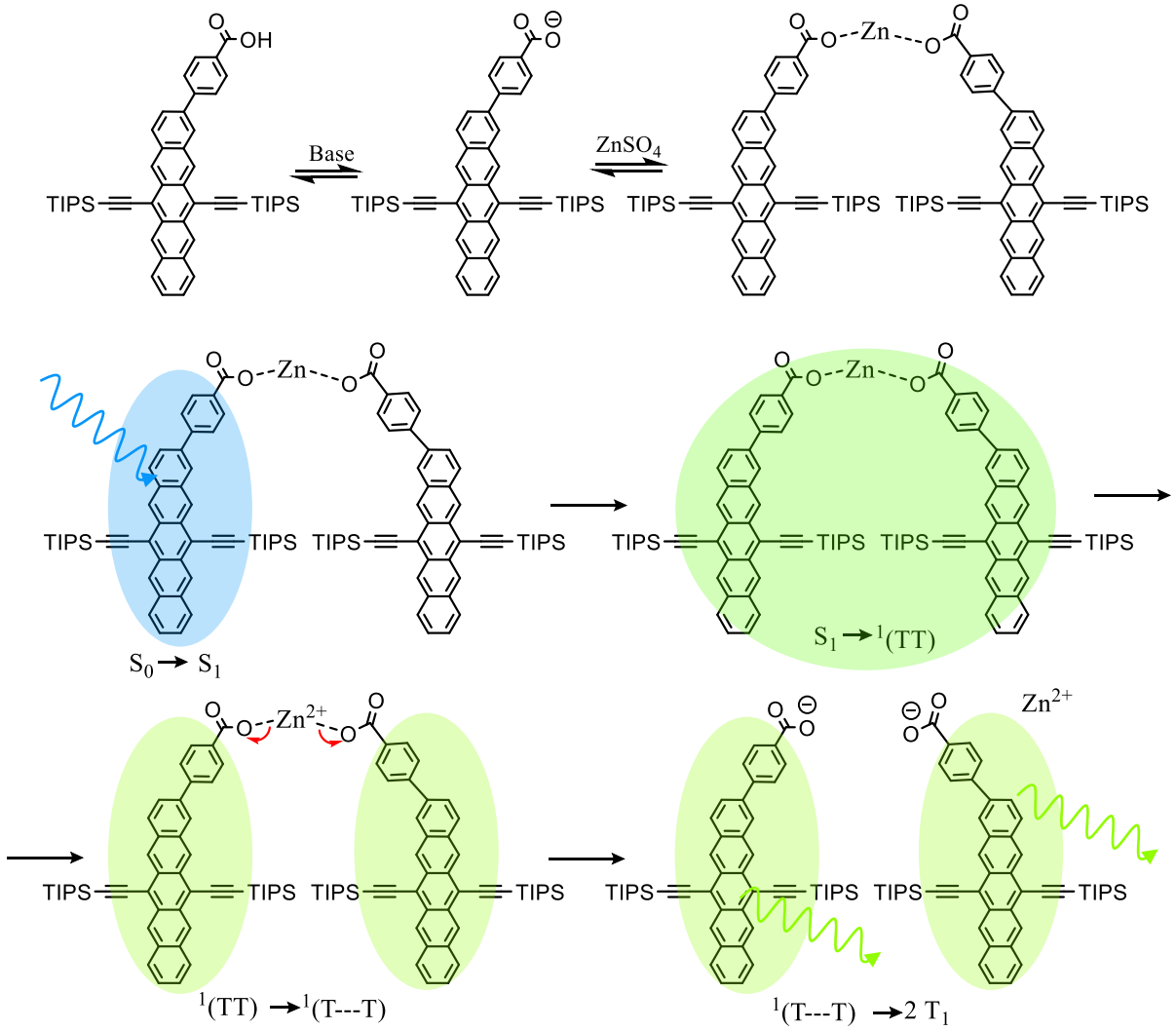

Figure 4 *Schematic figure of the proposed propagation of SF for a PCA-Zn complex. First deprotonation of the carboxylic acid. Secondly, formation of a complex after the addition of a cation. Thirdly, excitation of one of the chromophores that transitions into a triplet-triplet electronically coupled state, two separated triplet states that later can be depleted e.g., through phosphorescence of two photons. Dissociation of the cation results in two free chromophores that can separate.*

In Figure 4 the hypothesis for how the dynamic ion-ion bridges can facilitate SF is presented together with the proposed mechanism. First deprotonation of the carboxylic acids on the chromophores occurs, forming a negative charge on the chromophore. Thereafter, complexes with chromophores and a cation are created, Zn^{2+} is used here as an example. The weak ion-ion bonds can be seen as a dynamic bridge between the chromophores as they can associate and dissociate back and forth. When one of the chromophores is excited to S_1 the intent is that a ^{1}(TT) state can be created over the whole complex followed by formation of two separate triplet states, T_1, on the two chromophores. If the cation dissociates before the T_1 decays, separation of the triplets can be achieved. Decay pathways could either be by phosphorescence as shown in the figure but could also be non-radiative decay or through energy or electron transfer.

Several examples of where covalent bridges are used between the chromophores to facilitate SF can be found in the literature [23, 25]. A bridge separates the acceptors which can help with decreasing the likelihood for TTA. It can also change the energy levels, both the ground state and the excited states [26]. However, by forming a dimer by covalently bind the chromophores together the triplets can never be separated, so the energy must be utilized elsewise.

2.3 Ion-ion interactions

In order to investigate if SF can occur in a system similar to that presented in Figure 4 a complex must first be formed and knowledge about its properties gathered. In the following sections some theory about ion-ion interactions will be presented. The chromophores are not soluble in water, another solvent must therefore be used. Some alterations to what can be considered as basic chemistry theory must therefore be considered. Thus, first some background about deprotonation in non-aqueous solutions will be given.

2.3.1 Deprotonation in non-aqueous solutions

For weak acid and bases, an equilibrium between the protonated and deprotonated species is present. An equilibrium constant, K_a, can be used to describe the ratio of the acid and base forms, see Equation 3.

$$K_a = \frac{[B^-][H^+]}{[HB]} \tag{3}$$

where $[HB]$ is the concentration of the protonated acid form, $[B^-]$ is the concentration of the base form, and $[H^+]$ is the concentration of protons. The equilibrium constant gives a value of the acidity of the compound. However, in non-aqueous solvents the proton donating ability is affected compared to aqueous solutions [27]. Determination of the acidity can be made by titration and observation an inflection point [28, 29]. A second inflection point has been reported that is believed to be an effect of carboxylic acid- anion complexes. Again, the operations are in non-aqueous solutions where the polarity often is reduced compared with water, forming charges can therefore be challenging. Because the activity is changed traditional methods like a pH-paper, or a pH-meter cannot be used to measure the degree of deprotonation. Instead, UV-Vis will be used as detection technique within this project.

2.3.2 Complex formation

Coordination complexes can be formed by Lewis bases coordinating to a metal center. The binding constant, K, for a complex can be derived as the equilibrium constant for the reaction R1 as in Equation 4.

$$xM^a + \mathrm{yL^b} \underset{k_r'}{\overset{k_r}{\rightleftarrows}} \left(\mathrm{M_x}L_y\right)^{a-b} \quad (R1)$$

where M is the metal, L is the ligand, M_xL_y is the complex, x and y are the stochiometric coefficients, and a and b are the charges. Moreover, the equilibrium constant can be expressed by the ration of rate constants, k_r is the rate constant for the forward reaction, k_r' is the rate constant for the backward reaction.

$$K = \frac{[M_xL_y]}{[M]^x[L]^y} = \frac{\mathrm{k_r}}{\mathrm{k_r}'} \quad (4)$$

2.3.3 Benesi-Hildebrand method

The complex and the binding coefficient are important to know for a potential chromophore-cation complex. Thus, an order higher than 1:1 and a dissociation rate higher than the TTA rate are desired, so that two triplets can be formed and separated. The binding coefficients can provide important information about which complexes are formed and at which ratio. H.A. Benesi and J. H. Hildebrand proposed a method in 1949 to calculate the equilibrium constant based on absorption [30]. The model assumes that the formed complex and only one of the free compounds absorbs at a selected wavelength. Thus, the detected absorption will depend on molar ratio of ligand and metal if the molar extinction coefficient of the complex (ε_{LM}) and ligand (ε_L) differentiate. Hence, an expression of change in absorption ΔA, concentration of the complex $[LM]$, and extinction coefficients can be generated and is presented in Equation 5, see Supporting Information S.2 for a full derivation of the classic and modified Benesi-Hildebrand methods.

$$\Delta A = [LM](\varepsilon_{LM} - \varepsilon_L)l = [LM]\Delta\varepsilon l \quad (5)$$

Hence, the concentration of the complex can be determined by measuring the change in absorption. In combination with Equation 4 and mass balance one can determine the equilibrium constant from this type of measurement. When a complex of higher order is present, an approach with a modified model is necessary, where the equilibrium constants needs to be iterated [31].

2.4 Solar energy

As previously mentioned, one large driving force to study SF materials is the possibility of increasing the efficiency of solar cells, resulting in increasing competitiveness in the energy market. Climate change, energy security, and increased sustainability are some identified driving forces for incorporating more renewable energies [32]. Even though it is somewhat outside the scope of this thesis, a brief summary of solar panels, and the social, ethical and ecological aspects of solar energy are herein highlighted.

2.4.1 Solar panels

The photovoltaic effect was first observed in 1839 by Becquerel, where a voltage is created by irradiating a material. In 1954 Bell Labs created the first PV with silicon with an efficiency of 4% [33]. Since then, much has happened, the best crystalline silicon cells in 2022 have efficiencies in the interval of 21.2-27.6 % [2]. There are several different types of PVs; mono- or polycrystalline, thin film, organic, polymer, and dye-sensitized solar cells [34]. Silicon solar cells are the most used, usage of high-performing multicrystalline silicon has resulted in increased efficiency over the last decades [35], more than 90 % of solar panels sold under the same period were of this type. In recent years, silicon-based solar photovoltaics have not only dominated the turnover within the solar panel sector, it has subjugated the whole renewable energy industry [36].

Silicon is a semiconductor with a band gap (E_g) of 1.1 eV. Hence, the energy required for an electron to be excited and go from the valence band to the conducting band is 1.1 eV (1130 nm). Restricting the efficiency of power conversion as well as energy level that triplets need to have if a SF material would be incorporated with a solar panel.

A semiconductor is used in a solar cell to absorb the irradiating sun light to exceed the band gap. Usually a p-n-junction is used, hence a semiconductor that has been doped with donor and acceptor atoms. The band gap can through this be decreased and charges are more easily transported [37]. An illustration of a simplified solar panel can be seen in Figure 5. Irradiation leads to excitation where an electron and an electron hole are created in the depletion region. By transportation throughout the material and a following load, recombination can occur, and a current is created[38].

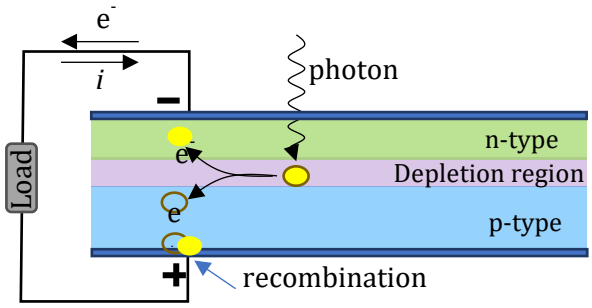

Figure 5 *Illustration of a solar panel, irradiation leads to excitation and creation of a negative electron and a positive electron hole. These are separated and a current flows through a load. Recombination occurs with the electrons and the electron holes.*

There are several energy losses within the solar panel, they can be divided into intrinsic and extrinsic losses. Where the extrinsic losses are external, and intrinsic ones are based on the semiconductor itself. Examples of the latter are thermalization due to vibrational relaxation, emission losses, and that the bandgap cannot be overcome as it is higher in energy than the main part of the irradiation [11]. Moreover, the temperature of the panel is important because an increase in temperature will reduce the band gap and therefore reduce the voltage drop and efficiency [34]. Hence by incorporation of up- or downconvering materials below band gap energy losses and thermalization can be reduced [11, 39].

2.4.2 Societal, ethical, and ecological aspects of solar energy

An increase in the electricity production from solar energy can have a positive impact by reducing the emission of greenhouse gases. Moreover, decreasing the dependency of fossil fuels. The transition can be initially costly, but levelized cost of energy forecasts that renewable systems will have significantly lower costs compared to fossil fuels and nuclear energy [40].

Solar energy has the advantage that it is available all over the world. Thus, it has the possibility to provide renewable and reliable energy globally [41]. Increasing the efficiency of solar panels decreases the area and material needed for the same amount of produced power, making it more resource effective. However, specific materials and techniques are still needed. According to Koese et al., material efficiency will be one of the most vital aspects in developing new solar panels. Along with material selection and recyclability [42]. The installations of PVs have increased during the last decade and are forecasted to continue. The cost reduction in the last decade, from 4731 $/W in 2010 to 883 $/W in 2020, substitutional social-economic impact, and inclusion of solar power in multiple strategies and plans globally indicates a large increase in the use of them[43].

However, the environmental and economic aspects of PV are not one-dimensional, there are multiple factors to consider. In a study where the power generation cost, environmental impact, and environmental external cost are compared between solar PVs and coal-fired power plants by Huang et al. is it showcased that the production cost of solar PV power is higher than for coal-fired power, 0.08 $/kWh and 0.05 $/kWh respectively. Production of PV cells will cause fossil consumption and hence lead to climate change but not to the same extent as for the coal-fired plants. The monetized environmental impact is 3.47 $/kWh for solar PV power and 116.20 $/kWh for coal-fired power. Furthermore, all the environmental impact categories are lower for PV compared to coal except for the metal resources consumption [44].

2.5 Experimental techniques

The following sections will present the background of vital techniques used within the project. First some general theory and equations are presented, followed by a description of the techniques.

2.5.1 Absorption

As previously mentioned, molecules can absorb light with specific wavelengths depending on the corresponding energy levels. The absorption of a sample can be measured by comparing the intensity difference before and after light passes through a sample. The intensity of the light before the sample, I_0, and after, I, are compared, and the absorption, A, can be calculated by Equation 6.

$$A = log\left(\frac{I_0}{I}\right) \tag{6}$$

Absorption at a wavelength, λ, means that the molecule has an energy transition that corresponds to the energy of the photon. A relationship between absorption and concentration of the chromophore was presented by Lambert and Beer, commonly called the Lambert-Beers law presented in Equation 7.

$$\mathrm{A} = \varepsilon \mathrm{cl} \tag{7}$$

where c is the concentration of the chromophore, l is the path length that the light travels, and ε is the molar extinction coefficient which is specific for the molecule and the wavelength[16].

The absorption can be measured at steady-state or be time-resolved. In the following sections, two examples of different techniques will be presented, UV-Vis absorption, and transient absorption.

2.5.1.1 Steady-state absorption

The steady-state absorption of a sample can be assessed by measuring the transmission of light through a sample. The light produced by a light source reaches a monochromator, the light proceeds to a sample and a following detector that detects the light intensity I. Comparing I to

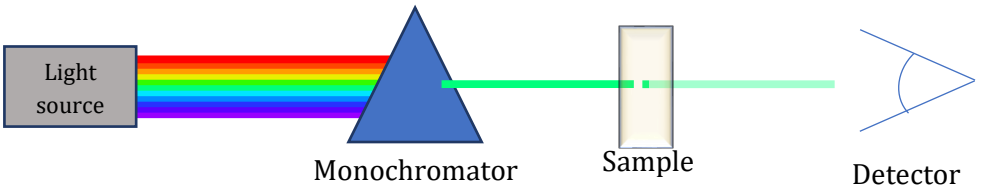

Figure 6 *Illustration of a UV-Vis spectrophotometer, the light produced by a light source goes through a monochromator, a sample, and reaches a detector.*

the intensity of beam that doesn't go through the sample, I_0, will give the absorbance of only the sample. It is the transmission that is detected rather than the absorption itself. Dependent on which radiation is used, different steady-state absorption spectra can be acquired. For the detection of electronic transitions, the UV and visible regions are utilized (λ=100-700 nm). In Figure 6 a schematic illustration of a UV-Vis spectrophotometer can be observed.

2.5.1.2 Transient absorption

The time dependency of excitation and subsequent decay of a system can be measured by using a technique called transient absorption (TA). Processes on the nanosecond to sub-picosecond level can be detected; determined by the setup used. Hence, processes such as SF can be detected by observing the progression of singlet formation followed by formation of triplets.

Without photoexcitation, a system is at its ground state (GS), and the electrons with the highest energy are at the highest occupied molecular orbital (HOMO). A weak probe beam can excite a fraction of the electrons to an unoccupied molecular orbital, to an excited state (ES) and absorption can be detected as previously explained. Let denote this as ground state absorption, A_{GS}. At time zero, a pulsed laser beam, called a pump beam, with a frequency, f, is exciting the sample. A high, non-equilibrium population of the excited states is created as a result. Hence, the Boltzmann distribution law is no longer valid. At times t>0, or t=τ, the probe beam is exciting the sample and the absorption is detected. τ is the delay from the excitation of the pump to the detection of the excitation via the probe. However, now both absorption from the excited state to higher excited states, excited state absorption (ESA), and absorption of the ground state can be detected. Because the population at the ground state is reduced at t=0, compared to before the pulse beam, t<0, a reduction of A_{GS} will be detected, called ground state bleach. Moreover, stimulated emission can also be detected as a result from excitation. It appears if the sample fluoresce as the excited states decays back to the ground state. Figure 7a schematic of a simplified TA setup can be seen. Figure **7**b showcases an illustration of electronic transitions occurring at the different times.

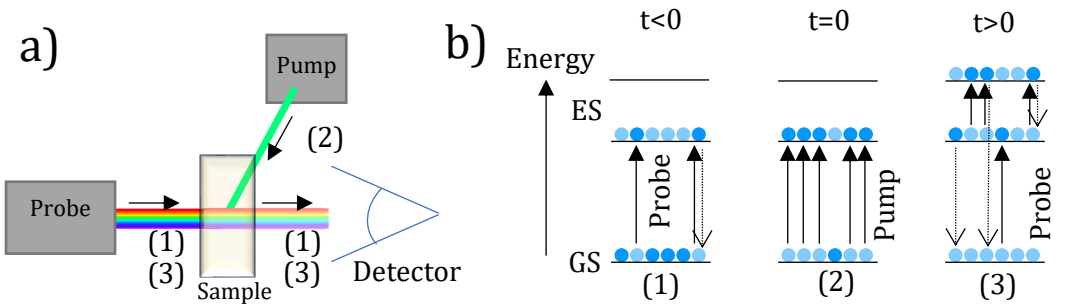

Figure 7 *Schematic of a transient absorption experiment a) illustration of TA setup with a continuous probe beam with intensity I_0. b) the energy levels involved at time t<0, t=0, and t>0, GS stands for ground state and ES for excited states. At (1) the sample is probed from the ground state to an excited state. At (2) the pump is added and a non-equilibrium state where the population at excited states are increased, at (3) excited state absorption is possible, exciting the electrons to higher energy states.*

A difference spectrum can be created, ΔA, where the absorption before and after the pump is evaluated. The absorption at time 0, $A(0)$, and t, $A(t)$, can be decided from Equation 6. ΔA can be calculated according to Equation 8.

$$\Delta A = A(t) - A(0) = \log\left(\frac{I_0(t)}{I(t)}\right) - \log\left(\frac{I_0(0)}{I(0)}\right) = \log\left(\frac{\frac{I_0(t)}{I(t)}}{\frac{I_0(0)}{I(0)}}\right) = \log\left(\frac{I_0(t) * I(0)}{I(t) * I_0(0)}\right) \quad (8)$$

The intensity of the probe beam is assumed to be constant, thus $I_0(t) = I_0(0)$. Therefore, by simplify Equation 8 the difference spectrum can be defined as in Equation 9.

$$\Delta A = \log\left(\frac{I(0)}{I(t)}\right) \quad (9)$$

Hence, only the intensity before and after the pump needs to be recorded to obtain the difference spectrum. In Figure 8 an illustration of the experimental setup used can be seen. The detection, by either a CCD camera or a PMT detector, starts at different delays after the sample been excited by the pump pulse. The delay, number of scans, and grafting are all parameters that can changed to obtain different measurements. Measurements with and without the pump can also be done simultaneously to obtain the intensities $I(0)$ and $I(t)$ at the same time if another experimental setup is used with two detectors and a split probe beam.

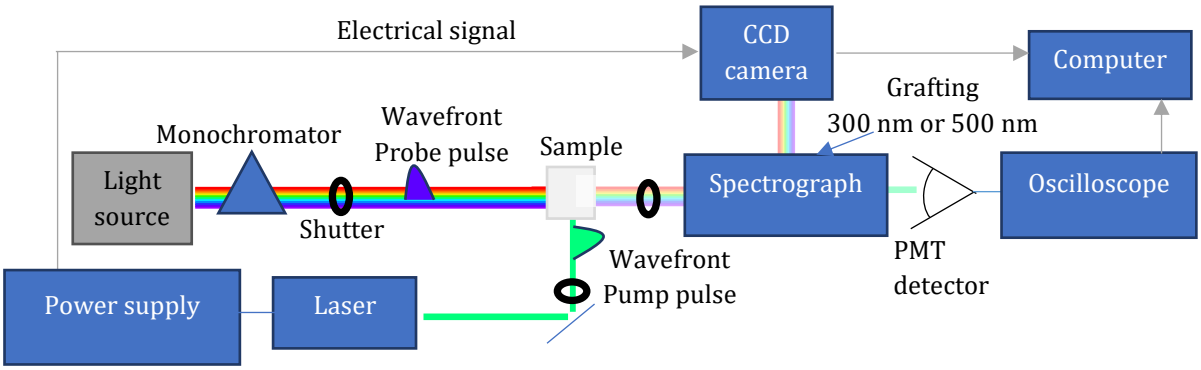

Figure 8 *Schematic illustration of transient absorption setup. The probe pulse and the pump pulse have an interval between them where the white light is delayed with τ. The delay is increased, the measurement is repeated. Either the CCD camera or the PMT can used as detector.*

The delay can be altered and a dependency of wavelength and time on the absorption can be obtained, ΔA(λ, τ). Thus, progressions can be detected with different rates and at various wavelengths. At sufficient τ, ΔA will be zero as the sample relaxes back to its ground state. Positive features of ΔA originate from ESA, negative peaks evolve from emission or ground-state bleaching. The technique's strength is that non-emissive states and dynamic photophysical processes can be detected [45]. The spectrum can also be emission corrected by only using the laser pump to measure the signal and then compare it to a dark background.

2.5.2 Emission

Emission provides valuable information that the absorption cannot give. In previously mentioned techniques the transmission difference forms the foundation of the detection mechanisms. For emission detection, the sample must be excited first, whereby the radiative decay can be detected. As for the absorption, emission can be detected at steady-state or time-resolved.

2.5.2.1 Steady-state emission

The steady-state emission can be measured in a fluorometer, see Figure 9 for a schematic illustration. By illuminating a sample by a selected wavelength, the sample is excited. When relaxing to the ground state, the sample can emit, and the light can be detected by measuring perpendicular in a chosen wavelength interval. Hence, a spectrum where the emission intensity against wavelength can be constructed. If instead the detection wavelength is kept constant and the excitation wavelength are changed in an interval, an excitation spectrum is obtained. That should be a similar result as the absorption spectrum.

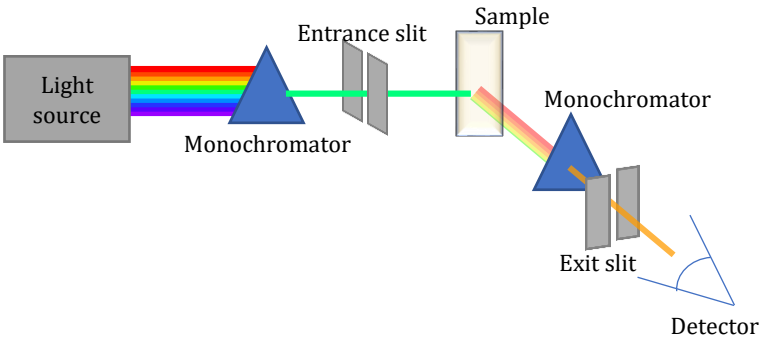

Figure 9 *Illustration of the most important parts of a fluorimeter. A light source produces light that goes through a monochromator to select an excitation wavelength. Entrances slit can be changed to control how much light that reaches the sample. The sample gest excited, and in a 90-degree angle from the incoming light the emitted radiation can be detected. It goes through a monochromator; an exit slit and lastly reaches a detector.*

2.5.2.2 Time-resolved emission

Time-resolved emission contains more information than the steady-state emission, subsequently can be more complicated to analyze. Static and dynamic quenching can in some cases be differentialized, and emission lifetimes can be determined to name a few advantages. Time-correlated single photon counting (TCSPC) is the most used for time-domain measurements and will be explained in more depth.

A sample is illuminated by a pulsed laser that excites it, the time it takes between excitation and a photon is emitted and reaching the detector is recorded. The detection rate is less than one photon per hundred excitations, meaning that single photons can be sensed. The counts are added together in a histogram, where the time is on the x-axis and the number of phonons in that time slot is on the y-axis. Each excitation pulse results in less than one photon detected due to dead time in the electronics in the PMT detector. Due to this, the histogram represents the waveform of decay [18]. By fitting the histogram to an equation similar to Equation 10 the emission lifetime can be calculated. t_n is a time parameter and is equal to the lifetime of the excited state. A_n is a preexponential factor and gives an indication of how dominant the decay with that rate is.

$$y = A_1 e^{-\frac{x}{t_1}} + A_2 e^{-\frac{x}{t_2}} + \ldots \tag{10}$$

2.5.3 Isothermal titration Calorimetry

Isothermal titration calorimetry, ITC, is a technique widely used within biology and biochemistry to determine binding coefficients and energies, often for proteins or large drug substances. Lately, the usage in more chemical applications has increased [46, 47]. It is based on temperature difference resulting from an association or dissociation event when a titrant is added in steps to a solution containing a host molecule that can interact with the titrant. A schematic picture of a general ITC setup can be observed in Figure 10.

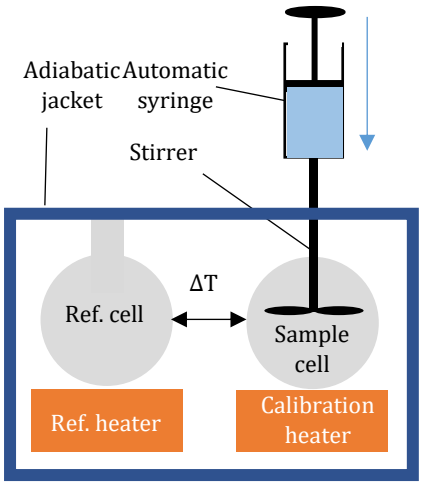

Figure 10 *Schematic diagram of an ITC instrument. A titrant is added by an automatic syringe, where the addition volume, duration and spacing can be programed, to a sample cell containing a known volume and concentration. Interaction between titrant and host molecule will change the temperature in the sample cell. Hence, the required power for maintaining the same temperature in the sample cell and a reference cell with the same solvent will be different. An adiabatic jacket is surrounding the cells, the power difference over time is collected.*

The temperature in the sample cell should be held constant as in a reference cell with the same solvent. The power needed to maintain the same temperature is recorded over time (µcal/s). The power is equal to the energy released in an exothermic process or absorbed in an endothermic process. The heat, Q, absorbed or evolved is proportional to the number of associations during the calorimetry titration and can be expressed as in Equation 11.

$$Q = V_0[M]_t \sum_i \frac{n_i \Delta H_{b,i} K_{a,i}[L]}{1 + K_{a,i}[L]} \tag{11}$$

Where V_0 is the cell volume, $[M]_t$ the concentration of host molecule in the solution, ΔH_b the binding enthalpy, K_a the binding constant, $[L]$ the concentration of ligand in the titrant, and n_i the number of binding sites where ligands independently can bind [48].

The binding coefficient and the enthalpy can be derived from the ITC measurement, hence the Gibbs free energy, ΔG, and the entropy, ΔS, can be also be decided if the surrounding temperature is known, see Equation 12.

$$\Delta G = RTln(K_a) = \Delta H - T\Delta S \tag{12}$$

3. Materials and method

The materials and methods used within the project will be presented in the following sections.

3.1 Materials

Nitrogen in-house; argon, 9-anthracenecarboxylic acid (ACA) 99% by Sigma Aldrich; 4-(6,13-bis((triisopropylsilyl)ethynyl)pentacene-2-yl)benzoic acid (PCA) synthesized before project; ethanol 95% analytical grade from Sloveco; acetonitrile >=99.8% from Fluka; dimethyl sulfoxide (DMSO), from Honeywell; acetone from Fisher Scientific; tetrabutylammonium hydroxide (TBAOH) in methanol by Sigma-Aldrich; diazabicycloundecene (DBU) from Sigma Aldrich; $ZnSO_4 \bullet 7H_2O$ 99.5 % from Merck; NaOH from Emplura; $MnSO_4$*monohydrate from Fluka Chemicals, 250 g, >99.0%; $MgSO_4$ hydrate by Sigma Aldrich, 1 kg 99-101 %; Na_2SO_4 from Merck, 2.5 kg; aluminum sulphate, $Al_2(SO_4)_3$, from Sigma-Aldrich Sweden AB, platinum octaethylporphyrin 2,3,7,8,12,13,17,18-octaethylporphyrin-22,24-diide (PtOEP) solution prepared in toluene.

Septum 12.9 mm SI/PTFE 70˚ by VWR, quartz cuvettes in the size of 10x10 mm, 4x10, and 2x10 mm from StarnaScientific.

3.2 Method

The preparation of samples, experimental setup for different techniques, and data analysis are presented in the following sections.

3.2.1 Sample preparation and titrations

Stock solutions were prepared by weighing a desired mass on a scale by Sartorius with the sensitivity of 0.000001 g, dissolved by adding solvent measured by an auto-pipet or measuring-flask. The solutions were sonicated for 10 minutes if not visibly dissolved. The solutions were labeled and stored until used.

Anaerobic samples were prepared by the following method: a cuvette with screw cap with a rubber septum was used. Parafilm was put around the edge of the cap, nitrogen gas was flooded through the sample for 15 min.

To a sample of chromophore were different additions of salts and base added in steps. A potential change was detected by some or several of the following detection techniques.

3.2.2 Steady-state absorption

The absorption was measured by a Varian-Cary 50 Bio UV−vis Spectrophotometer in the interval 800-200 or 1100-200 nm with the setting fast and baseline corrected. Pure solvent was measured as the first measurement conducted with each new set of samples and was saved as the baseline. Titration measurements were performed by repeatedly adding a small amount of base or cation solution to a chromophore sample and measuring the steady-state absorption.

The molar excitation coefficient for ACA and PCA in different solvents were determined by titrating a small amount of chromophore (ACA in DMSO, PCA in acetone, and PCA in acetonitrile) with known concentration to the respective solvent.

3.2.3 Transient absorption

Two different type of transient absorption (TA) measurements were performed, nanosecond and femtosecond. The latter was only used to produce preliminary data and will not be further discussed.

The experimental setup for the nsTA measurements has previously be presented, see illustration in Figure 8. A laser by Spectra-Physics and the model Quanta-Ray connected to a PrimoScan were turned on. The wavelength was set to 450 nm and the outlet power were measured and noted, in the range of 130-180 mV. The white light source used was a halogen display/optic lamp by Osram in an Oriel Instruments Universal QHT/IR lamp housing by A Newport Corporation Brand. The lamp was ramped up to 250 mW. The CCD camera by Andor and the model iStar was started, and it was made sure that the cooling worked. The wavelength on the laser was changed to desired excitation wavelength (415, 600 or 536 nm), a degassed sample was placed in the sample holder. Software made in Labview was stated. For the most experiments a CCD camera was used as detector, on some occasions a PMT was instead used.

Obtaining a spectrum: the CCD camera was cooled to a temperature of -20 °. The 500 nm grating in the CCD camera was selected, average 100, step size and number of steps were selected dependent on which run was made. Prior, an average of 20 was used where the step size and number of steps were changed until a setting was found where the growth and depletion of the sample could be observed. The gain was selected to have high intensity at the first measurements without damaging the detector.

Obtaining a decay trace: The PMT and an oscilloscope of type Tektronix TDS2022 were stared. The power to the PMT was selected. An average is selected with the base of 16 and a detection wavelength is selected.

Triplet sensitization was achieved by adding PtOEP to the chromophore and the sample was excited at 536 nm. A sample with only PtOEP was measured.

3.2.4 Steady state emission and excitation

The fluorescence was measured by a spectro- fluorometer, Spex Fluorolog 3 from JY Horiba with a PMT detector of the type Photoeod™ series, model PC177CE005. The entrance and exit slits were kept equal. Initially, a real-time-measurement was performed to find appropriate condition to obtain a good signal-to-noise ratio without surpassing 10^6 counts. The excitation wavelength for ACA was kept at 377 nm, for PCA 377 nm and 600 nm was used. Excitation spectra were collected at 415, 465 nm for ACA, and at 432 and 672 nm for PCA. A built-in correction file was used to adjust for instrumental error.

3.2.5 Time-correlated single photon counting

An Edinburgh Instruments LifeSpec II is used for the TCSPC measurements. The cooling for the PMT detector was set to -18 ˚C. The detector used was an MCP-PMT. A diode by the brand PicoQuant was then started, the alignment of the diode was changed manually by measuring the signal near the laser diode's wavelength with a scattering plate and the iris set to 1 until a high signal was obtained. The instrument response function (IRF) was measured using a scattering plate. A degassed sample was then placed in the sample holder, the iris was changed until a signal 10 % of the frequency was detected or fully open. The diodes used were of the wavelength 377nm, 405 nm and 560 nm. 10 000 counts were used as a stop condition for most of the experiments if not the detection time exceeded 2 hours. Then the stop condition then was lowered.

3.2.6 Isothermal Titration Calorimetry

A MicroCal iTC200 MicroCalorimeter were used, normally only aqueous solutions are used with the equipment, hence some extra precautions were needed to be made. The Hamilton syringe and cells were rinsed with DMSO before and after measurements. Moreover, they were cleaned

manually with water before the automized cleaning process could be performed to not damage the tubing with DMSO. The settings were alternated until a satisfactorily measurement was obtained, the final programing used were 39 additions, 0.5 µl per addition during 2 s, high gain, 120 s between additions, and 750 RPM stirring speed. An experiment matrix was built up by titration of different possible combinations. A thermograph, the power required plotted against the time was obtained. Between each addition equilibrium should be reached. As a first measurement each day a baseline with addition of solvent in solvent was performed. Between each measurement, the sample cell was manually rinsed before a new sample was added.

3.2.7 Data analysis

The absorption at 365 nm for ACA, and at 645 nm and for PCA were plotted against the concentration of chromophore. A linear regression was made, the slope being the extinction coefficient, ε.

The separate steady-state absorption, emission and excitation spectra from the additions were volume corrected to normalize the chromophore concentration throughout the titration. The volume correction was performed by multiplying the detected value with a factor of $\frac{V_{added}+V_{inital}}{V_{initial}}$ to correct for dilution effects. Titration spectra was created for each titration by combining all the measurements from respective technique and sample.

Modelling of the complex formation based on Benesi-Hildebrand method was conducted as following. The absorption at 377 nm for the titration of addition of $ZnSO_4$ to ACA deprotonated with DBU was plotted against the concentration of added Zn^{2+}. Three different complex formations were proposed, a 1:1 complex, a 1:2 complex with irreversible binding, or a 1:2 complex with reversible binding. In the two formers, the $\varepsilon_{complex}$ was extrapolated from the last data point where it was assumed that all ACA was part of a complex and all absorption originated from the formed complex. The concentration of complex, and hence free ACA and Zn^{2+}, could be derived from Equation 5. The concentrations were plotted against the number of additions and a graphical analysis was executed. For the reversible complex formation, it was assumed that in the later additions the reaction $ZnACA_2 + Zn^{2+} \rightarrow 2\,(ZnACA)^+$ was dominant, and a linear regression could be conducted according to Equation SI.2.14. See Supporting Information S.2 for full derivation.

The onset of the decays from the TCSPC measurements were corrected according to the onset of the IRF and a new time zero was set. The decays were fitted to a mono-exponential or biexponential equation dependent on which gave the best fit.

The endothermic part of the signal from each addition from ITC was integrated, plotted against the molar ratio resulting in a Wiseman plot (also called the ITC titration curve[47]), some outlines were removed. A non-linear regression was iterated, see Equation 13, by the software MicroCal Analysis, determining $n, \Delta H_b$, and K_a [48], see Supporting Information S.3 for derivation of expression.

$$Q = \frac{n[M]_t \Delta H V_0}{2}\left[1 + \frac{[L]_t}{n[M]_t} + \frac{1}{nK_a[M]_t} - \sqrt{\left(1 + \frac{[L]_t}{n[M]_t} + \frac{1}{nK_a[M]_t}\right)^2 - \frac{4[L]_t}{n[M]_t}}\right] \qquad (13)$$

4. Results and discussion

The results obtained are presented and discussed in the following chapter. The overall aim is to create a system where dynamic ion-ion bridges are formed and so that one can study if SF can be facilitated in this manner. First a photophysical characterization of ACA and PCA are reported. Followed by results from deprotonation and how it affects the photophysical properties. A charge on the chromophores is needed for them to bind to a cation later and form a complex. Thirdly, results from ion-ion interactions between the chromophores and metal cations will be presented together with a modelling of a complex formation between ACA and zinc. The change in steady-state absorption and emission, transient absorption, and emission lifetime are detected and analyzed to gather knowledge for potential further studies of potential SF in chromophore-cation complexes with dynamic ion-ion bridges.

4.1 Photophysical characterization

In this section the photochemistry of the two chromophores, ACA and PCA, will be characterized to lay a foundation for the following discussion. Initially, the photophysical characterization of ACA will be presented.

4.1.1 Anthracene carboxylic acid

The steady-state absorption and emission was first investigated. In Figure 11, the absorption and emission of ACA in DMSO is shown. Absorption peaks are observed at 317, 334, 349, 366, and 386 nm, emission at 464 nm when exciting at 377 nm. Hence, it absorbed in the UV region and appeared transparent to the naked eye. Previously, a concentration dependency affecting the absorption has been reported, originating from the formation of dimers of ACA with its carboxylic acids facing each other [49, 50]. A concentration dependency has not been observed in this project and investigations of it has not been within the scope. However, the lack of vibrational resolution in the emission spectrum can be explained by the formation of dimers. When a dimer of ACA is excited and then interacts with another dimer in its ground state an excited tetramer is formed, resulting in a broad fluorescence [49].

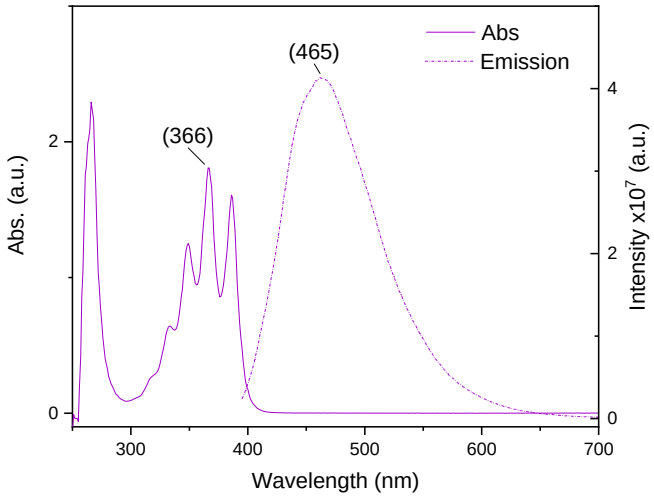

Figure 11 *Absorption and emission of ACA in DMSO, excitation wavelength 377 nm.*

The molar excitation coefficient was determined to be 7950 cm^{-1} M^{-1} at 365 nm in DMSO by titration and fitting to Lambert-Beers law. The emission lifetime was ascertained to be 11.7 ns at

465 ns by a mono-exponential fitting to the decay collected from a TCSPC measurement, see Supporting information S.4 for the fitting, and Table 1 for comparison of other decays.

In Figure 12 a spectrum of transient absorption for ACA in DMSO is presented. At around 445 nm a negative peak can be seen that decays within 100 ns. It is close in both shape and energy to the emission from ACA, However, the decay time for this peak was determined to be 22 ns by a mono exponential fitting compared to 11.7 ns from the TCSPC measurements. In addition, the steady-state emission was detected at 465 nm. This will be further discussed in section 4.4. The sample was probed with a laser with excitation wavelength 415 nm compared to 377 nm used for the steady-state emission. Examining the steady-state absorption in Figure 11 one can conclude that the absorption is quite low at 415 nm. However, it was selected based on the equipment used for the TA where different pathways are used for visible and UV light. The OPO could not select UV light or values lower than 410 nm. Therefore 415 nm was selected to avoid the large power drop near 412 nm.

No positive signal could be seen in Figure 12, indicating that there was no absorption of excited states. This may nevertheless not be true as it could be overlapping with the substantial emission around 450 nm and would therefore not be detectable. The molar extinction coefficient of the ESA has not been determined, as no ESA was detected. However, if $\varepsilon_{ESA} << \varepsilon_{GS}$ it will always be difficult to detect. There was some indication that the emission peak decayed with different rates at different wavelengths, see Table 1. Hence ESA may be occulting at the same wavelengths as the emission. However, to confirm this higher time resolution experiments should be performed. The negative band seen at 200-300 nm was most likely a ground state blech as it depletes faster than the stimulated emission. The band at 900 nm is believed to be a doubling of the emission.

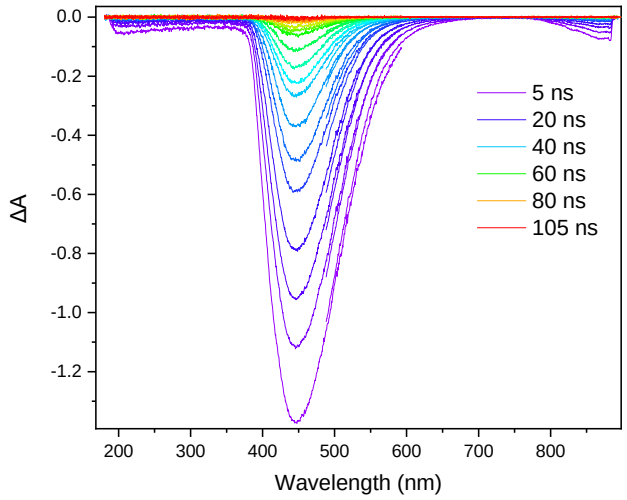

Figure 12 *Transient absorption spectrum of ACA in DMSO, excitation wavelength 415 nm.*

To potentially probe the triplet state of ACA, a sensitizer was added, platinum octaethylporphyrin 2,3,7,8,12,13,17,18-octaethylporphyrin-22,24-diide (PtOEP). First PtOEP without ACA was excited at 536 nm where peaks at 414 nm, 528 nm, and 640 nm could be observed, see Figure 13a. A sample with ACA and PtOEP was then measured, the resulting spectrum can be seen in Figure 13b. Three peaks could be observed at the first scan, at 414 nm, 528 nm, and 640 nm. These can all be assigned to PtOEP, after 6 µs a peak at 427 nm became visible while the others have decayed. The decay of PtOEP was faster when ACA was present compared to without it,

within 1 µs compared to more than 4 µs. Hence, ACA seems to quench PtOEP indicating triplet energy transfer from PtOEP to ACA resulting in ESA of ACA. No phosphorescence can be observed, implying that non-radiative decays dominate this state. Which energy level ACA has a triplet cannot be determined from this experiment. However, it can be stated that the triplet of ACA seems has lower energy than 1.9 eV (640 nm). Moreover, no features of pure ACA can be seen as there is no absorption at 536 nm. A long-lived triplet state is a requirement for downconversion through SF to be successful.

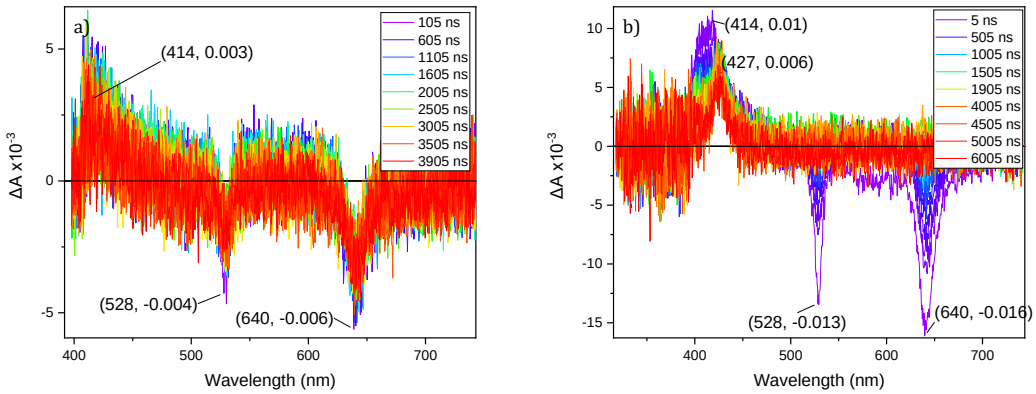

Figure 13 *Transient absorption spectra excited at 536 nm, a) PtOEP in DMSO, b) of ACA in DMSO with PtOEP added*

4.1.2 Pentacene carboxylic acid

The relative novelty of PCA results in a more complex analysis, hence, there are only a few previous results to compare with in the literature. Therefore, a comparison between unfunctionalized TIPS-Pentacene and PCA will be done with the assumption that the functionalization will not affect the photochemistry drastically.

4.1.2.1 Steady-state absorption and emission of PCA

In Figure 14 absorption of PCA in DMSO can be observed. Two different electronic bands can be seen, centering at around 600 nm, and 400 nm, vibrational transitions within the bands can be observed. Moreover, a sharp peak at 318 and at 276 nm can be observed. An overlap for between the bands >400 nm can be observed.

By convention, only the most redshifted bands are often presented and probed. The shape and position of the band at 600 nm presented in Figure 14 and in the work of R. Ringström et al., A. Maliakal et al., and F. A. Schaberle et al., are similar [24, 51, 52]. However, these experiments were conducted in toluene and THF, respectively, which could have some influence on the spectral shape and position. The band centered at 315 nm does not have similar shape to the vibrational modes as for the other two bands. Suggesting that this absorption could come from a different species and that there are possible some impurities in the sample. It should be noted that benzoic acid in water has been reported to absorb around 240 nm and the absorption maxima dependent on deprotonation grade [53].

PCA was excited at 377 nm and 600 nm and the emission normalized at 672 nm, Figure 14. When exciting at 377 nm, one emission band at 450 nm with two peaks can be observed, as well as a peak at 672 nm. The vibrational shape of the two band differs. Moreover, by having two different emission band Kasha's rule is not followed, which proposes that they arise from two different species. This strengthens the proposition that the sample has impurities. An NMR measurement was performed; however, the results are inconclusive due to too much noise. Hence, the structure

of the PCA has not been determined within this project. Most likely some degradation has occurred, consequently giving noise in the NMR signal. PCA was synthesized a few months prior the start of this project which could have leaded to degradation during storage. Recrystallization trials were conducted without result. When exciting at 600 nm only a peak at 672 nm was detected, similar in shape as when excited at 377 nm. The emission lifetime was determined to be 6.2 ns, see Supporting information S.5 for fitting and Table 1 for comparison with other decays.

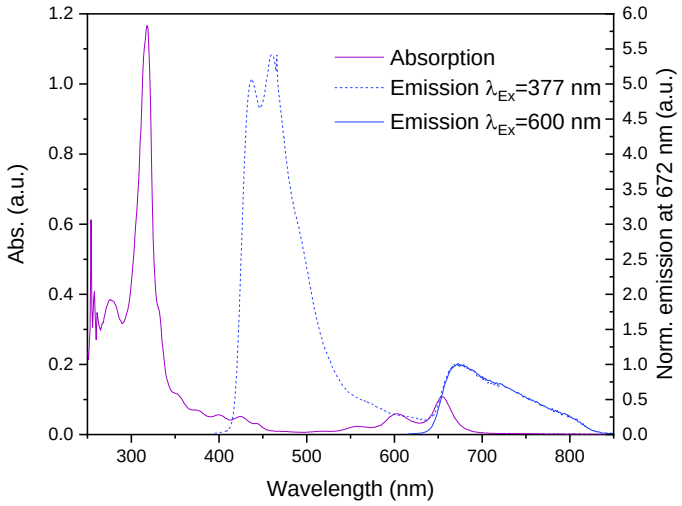

Figure 14 *Absorption and emission of PCA in DMSO. Emission from excitation with 377 nm is normalized at 672 nm to match the intensity from emission arising from excitation with 600 nm.*

4.1.2.2 Stability tests for PCA

The stability of PCA was investigated over a 12-day period, where the absorption was measured, see Figure 15a. The sample was kept in the dark during the stability test. A drastic increase between the first measurement and the second could be seen, probably due to a slow dissolution of PCA in DMSO. The following change over time was minor, with a small decrease in intensity over the whole interval. However, if normalized at 655 nm, one can see an increase at 277 nm larger compared to the overall spectra. Indicating that this could be the absorption of some degradation product.

Furthermore, the light sensitivity was investigated by illuminating a sample of PCA in DMSO with a Xe-lamp and absorption measurements performed in intervals over 1 hour duration and 0.6 W power. The result is presented in Figure 15b. A decrease can be observed at the band at 600 nm and at 317 nm, indicating a depletion due to irradiation. However, the absorption at 400 nm, did not decrease. Instead, a slight increase in absorption and minor red-shift could be observed. Furthermore, an increase in absorption at 279 nm was detected. No peak was constant during the stability analysis, indicating that the previously mentioned impurities rather was a depletion product originating from PCA.

Accordingly, the stability in solution can be seen as good and should not affect following measurement. However, the compound seems to be light sensitive, decreasing the detection accuracy as the chromophore concentration changes over time if light is used in the measurement. Thus, PCA is not a good candidate for incorporation to solar panels due to its low light stability. TIPS-pentacene is more used as a model system for investigating SF mechanisms and progression rather for practical applications. These results are therefore expected, but it is

important to remember when examining the following results that the concentration may differ during an experiment as it may degrade during a measurement or between.

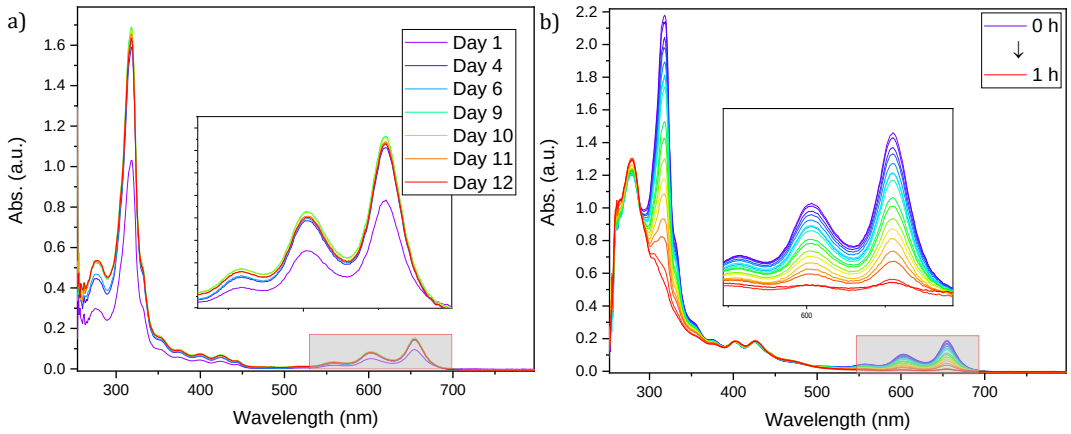

Figure 15 *Stability test of PCA where absorption spectra were collected, a) over a two-week period, b) between irradiation of a Xe-lamp with 600mW during 1 hour in total.*

4.1.2.3 Transient absorption of PCA

In an attempt of assigning the absorption bands to transitions, based on the literature and the stability tests. It is thought that they arise from right to left: the $S_0 \rightarrow S_1$ transition for the band at 600 nm, $S_0 \rightarrow S_2$ transition for the band at 400 nm, $S_0 \rightarrow S_3$ transition the sharp peak at 317 nm, and below 300 nm impurities, perhaps from benzoic acid, and/or unknown transitions from PCA.

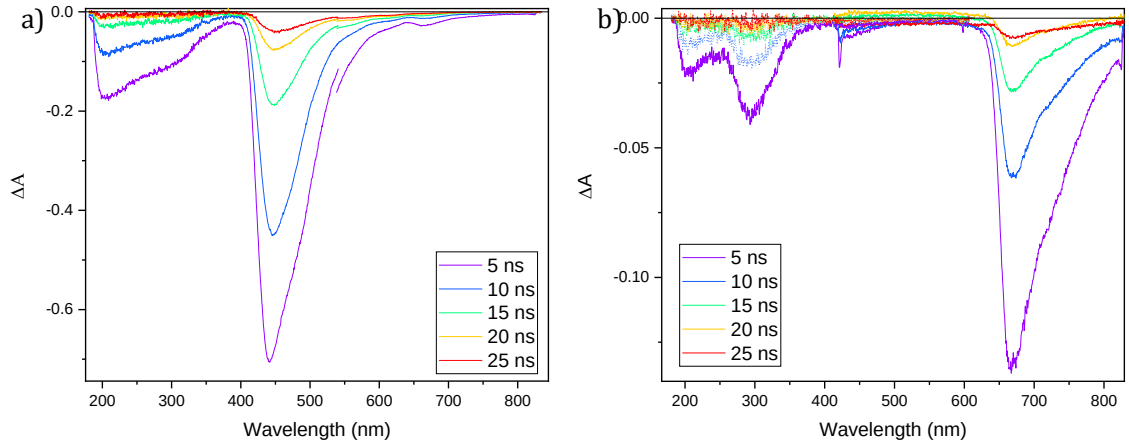

Figure 16 *Transient absorption of PCA in DMSO, a) λ_{Ex}=415 nm b) λ_{Ex}=600 nm.*

Transient absorption spectra of PCA are presented in Figure 16 with excitation wavelength 415 and 600 nm respectively. Decreasing intensities at 442 nm, 206 nm, with a shoulder at 314 nm, and 661 nm can be observed in Figure 16a. The peaks at 442 and 661 nm can be assigned to the emission bands, which was observed when exciting with 377 nm in steady state emission in Figure 14. Excitation at the wavelength 600 nm resulted in three different peaks, at 206 nm, 294 nm, and 669 nm. The later can be assigned to the emission observed in steady state at 672 nm. However, the two former peaks were more difficult to assign. It could be a ground state bleaching, but no absorption in the steady state has been detected that corresponds with these wavelengths. All three peaks deplete within 25 ns, with decay rates around 6 ns, see Table 1. As seen in Figure 15b the light stability was low, and the depletion observed from TA could be due to concentration

decreasing as the experiment progresses rather than lifetimes of the different states. A physical change from a light blue color to a pale yellow could be observed by eye in room light before and after TA measurements, most likely due to degradation during the measurement.

SF should be possible for pentacene's, but at high concentration and it is therefore not probable in this sample with low concentration. The peak at 206 nm is present in both excitations, indicating that it could either come from PCA, or that is an instrumental artifact. The latter is probable due to it is relatively close to the limit for the CCD sensitivity range and/or the low intensity from the halogen probe light in this range. Nevertheless, the intensity at this peak was substantial and should be taken into consideration. To gain as large interval as possible, two different scans with the CCD camera were done and plotted together, hence some overlap around 400-500 nm can be observed, as well as a sharp cut at 500 nm.

Moreover, the poor solubility of PCA have caused difficulties, where it decreases in this order acetone, acetonitrile, and DMSO. Hence, determination of the molar extinction coefficient has been troublesome as a concentration could not be established with high accuracy. Therefore, the concentration of PCA in the following experiments could be somewhat imprecise. However, attempts to calculate the molar extinction coefficient were performed and the results were; in acetone at 645 nm; $\varepsilon_{aceton,645nm} = 5820\, M^{-1}cm^{-1}$, and in acetonitrile $\varepsilon_{acetonitrile,645nm} = 2530\, M^{-1}cm^{-1}$. This will prove to be troublesome later, as if the concentration of the chromophore is unknown the amount of base and metal cations necessary to obtain a dimer complex or with higher order is also unspecified.

Sensitizing of the triplet energy in PCA was performed by adding PtOEP to PCA and excide at 536 nm, see TA spectrum in Figure 17. Three peaks can be observed, at 398, 565, and 669 nm. The peak at 669 nm was previously seen in Figure 16b when PCA was excited at 600 nm and was then assigned to be the emission from PCA. Hence, the peak at 669 in Figure 17 seems to also originate from the emission from PCA as PCA also can absorb at 536 nm. Moreover, it decays in a similar rate within the first 30 ns as for PCA without PtOEP.

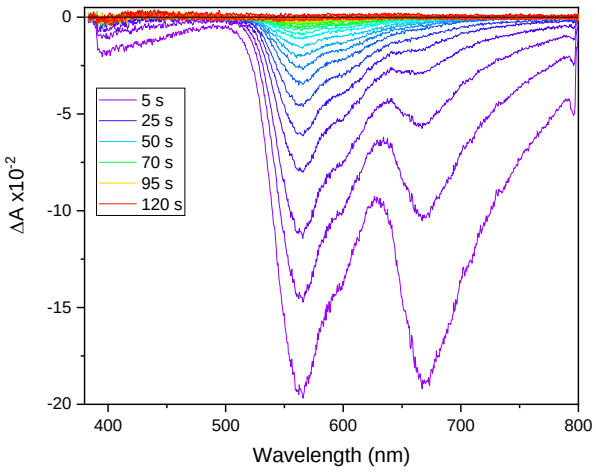

Figure 17 *TA measurement of PCA with PtOEP in DMSO, excitation wavelength 536 nm, traces from 5 ns – 125 ns.*

The peak at 398 could be a ground state bleach of PCA. It is possible that the peak was enhanced as it is close to the detection boundary. What was more interesting was the peak at 565 nm that has not been observed for either PCA or PtOEP previously. It decays slower than the emission

peak (depletes in around 80 ns compared to 30 ns) and is believed to be ground state bleaching due to energy transfer from the PtOEP to a triplet sate in PCA. Or at least that it is a proof of some type of process can be occurring with higher excitation levels. The phosphorescence was not detected, nor any ESA. However, the accessed energy state may have a non-radiative decay or be below the detection limit and can therefore not be detected. Information about the triplet state is important for further investigations about SF.

4.2 Deprotonation of the carboxylic acids

One conclusion from the previously conducted prestudy was that deprotonation of ACA seems to be an important prerequisite for the formation of complexes. Sulphate is a strong enough base to deprotonate ACA, but complexes with a higher ratio of ACA to cation seems unlikely if no other base is added. Hence, full deprotonation before addition of cation is desirable to form complexes where SF has the possibility to occur. In this section the results from additions of the bases DBU and TBAOH to ACA and PCA respectively are presented.

4.2.1 ACA with base

DBU was added to ACA in steps, the absorption and emission were measured between each step, presented in Figure 18 going from a 1:0 ratio to 1:2.5 of ACA:DBU. In the absorption a redshift can be observed and several isosbestic points resulting from the addition of DBU. Indicating that a reaction has occurred with a transition from one absorbing reactant to a product. In the emission spectrum a decrease in intensity can be observed as the concentration of DBU is increased. Moreover, a blueshift and more clear vibrational resolution was present. After 180 µl been added, a 1:1.5 ratio, no more changes can be seen in the spectrum, indicating that the solution was fully deprotonated. The increased vibrational resolution was believed to originate from that there no longer exist any ACA dimers in the solution as previously mentioned in 4.1.1 was the main reason behind the broad emission spectrum. Thus, the deprotonation of ACA adds a negative charge leading to increased spectral separation.

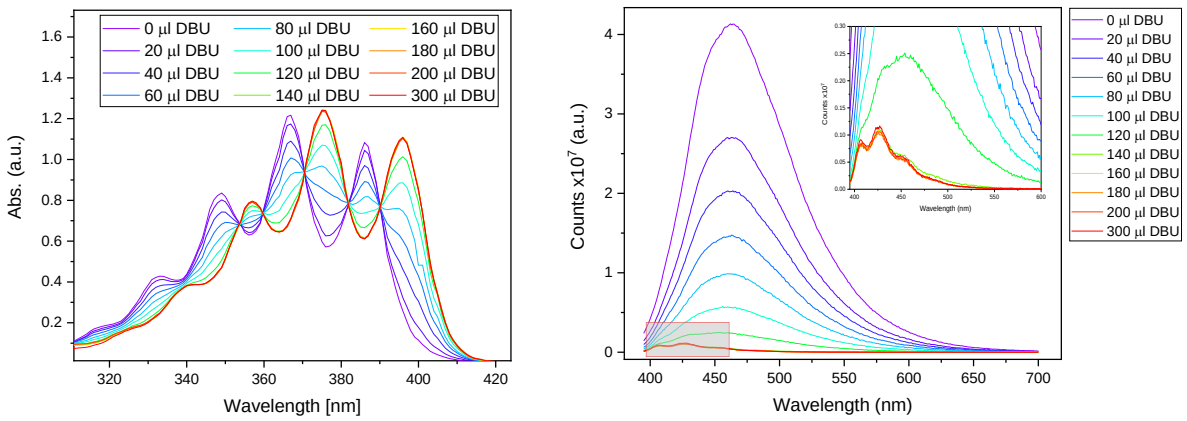

Figure 18 *Absorption (to the left) and emission (to the right) spectrum for titration of DBU to ACA in DMSO. Adding 300 µl DBU with concentration 0.35 mM to ACA with concentration 0.14 mM*

The emission lifetime was measured using TCSPC and the results are presented in Figure 19. It can be observed that the emission lifetime was decreased with increased DBU concentration. The emission lifetime for ACA without base was as previously mentioned 11.7 ns. Addition of DBU resulted in a lifetime <1 ns where the detection sensitivity made it impossible obtaining an accurate value as it is within the IRF. Hence, quenching seems to be more effective for deprotonated ACA. The reason behind this could be that the negative charge on the chromophore

destabilize the excited state, probing it to decay faster back to the ground state. Moreover, in Figure 19 two population can be observed when 120 µl of DBU was added, one that has the same rate as before (same slope) and one that is <1 ns. Thus, it can be concluded that a reaction with the DBU and ACA was occurring that was producing a short-lived species. In Table 1 the rates are displayed. Deprotonation with TBAOH showed similar result, see Supporting Information S.6. Supporting that it is the deprotonation of ACA that is the underlaying factor for the shifts in absorption, emission, and the fast decay, rather than quenching from the base. Due to the very fast decay, the detection limit of the used TA setup was exceeded. Hence, the transient development during deprotonation could not be investigated.

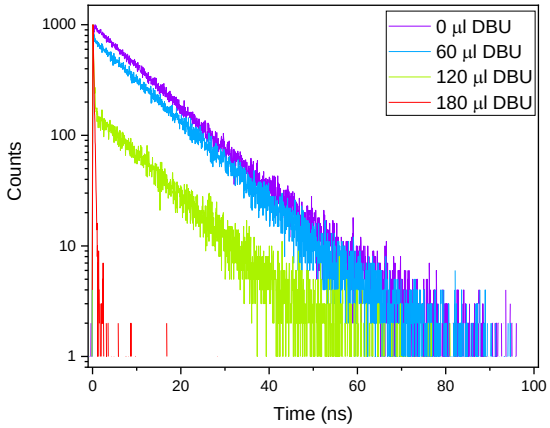

Figure 19 *Decay traces collected by TCSPC for addition of DBU to ACA in DMSO excitation wavelength 377 nm, detected at 465 nm.*

Furthermore, worth mentioning from these results; the degree of deprotonation of a chromophore can largely influence its photophysical properties. The quantum yield and emission lifetime decreased dramatically with increased deprotonation. The simultaneous redshift in absorption and blueshift in emission subsequently reducing the Stokes shift. Hence, the quantity of negatively charge chromophores can tune the energy levels and influence multiple other properties.

Quenching can be an indication of SF in a system, thus new decay processes with different rates are introduced decreasing the emission quantum yield. If deprotonation also leads to these effects, it may be difficult to detect potential SF in a later step. However, ACA does not fulfill the energetic requirements for SF but is rather used as a model system to design a chromophore complex.

4.2.2 PCA with base

DBU was added stepwise to PCA in DMSO, and absorption and emission spectra were collected after each addition, see Figure 20. The trend of detecting large shifts in emission and absorption caused by deprotonation observed for ACA could not be seen for PCA. A decrease in absorption and emission can be observed, note that it is not due to diluting effects as the spectra are volume corrected. After 40 µl 0.00165 M DBU had been added no more change in emission can be detected. Thus, a saturation may be reached where all PCA has been deprotonated.

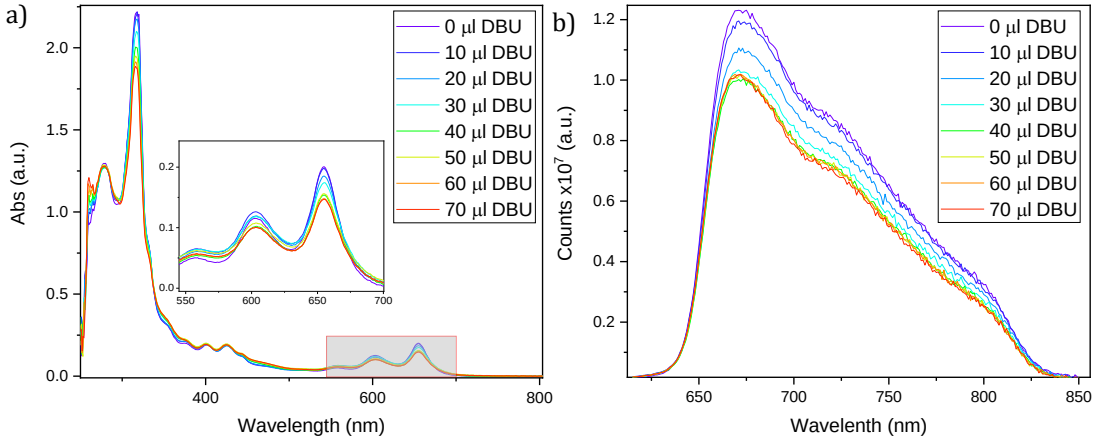

Figure 20 *Addition 0-70 µl DBU (1.65 mM) to PCA in DMSO, a) absorption b) emission with excitation wavelength 600 nm*

The effect on the absorption and emission of PCA in DMSO when TBAOH was added is presented in Figure 21. A decrease could be observed at 315 nm and the band at 600 nm gets broadened and depleted, simultaneously an increase at 400 and 265 nm was detected. The vibrational resolution at 400 nm was decreased, indicating that a new species was created and growing in, overlapping with the S_2 band. This could be a feature of deprotonated PCA, like the creation of new peaks for ACA. No clear isosbestic points can be observed. A clear decrease in emission intensity could be observed together with a redshift. The change in absorption resembles the light sensitivity study in Figure 15b. This could indicate that the signal from the PCA was decreased as a result to deprotonation or depletion throughout the experiment. However, the former tends to be more probable based on the large change in the emission form the first addition. Moreover, similar result when TBAOH added to PCA in acetonitrile was observed, see Supporting Information S.7.

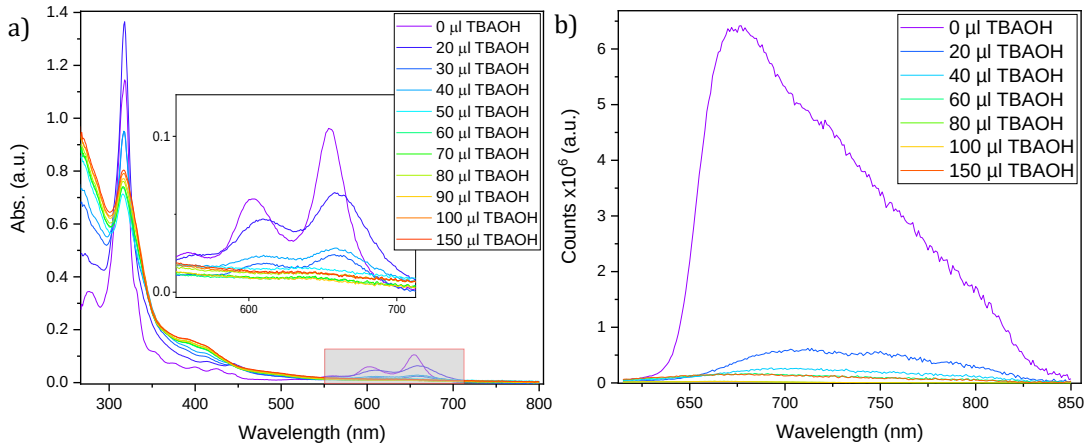

Figure 21 *Addition of TBAOH to PCA in DMSO, a) absorption b) emission with excitation wavelength 600 nm*

Three different explanations why no shifts in absorption could be detected similarly to deprotonation of ACA are proposed; (i) the structure of PCA where the acid is isolated from the chromophore results in small or non-detectable change in emission and absorption, (ii) the acid is not deprotonated by either OH^- or DBU, (iii) the synthesis of PCA has failed or PCA has

degenerated so that there is no acid to deprotonate. The pKa values for DBU and OH^- are 16.4 and 15.7, hence can be considered strong bases. Furthermore, deprotonation in nonaqueous solutions can be more complicated and pH loses some of its meaning. However, the probability that TBAOH should react in any other way than through deprotonation seems low. Hence, suggestion number two can be ruled out. As discussed in section 4.1.2 no clear evidence of impurities can be detected in the stability trials, and the characteristics are comparable to those of TIPS-Pentacene. Therefore, explanation (i) is considered as the most likely. Resulting in that a potential complexation with cations later may also have little influence on the photochemistry if not other processes become accessible due to the confined configuration.

The emission lifetime was measured with TCSPC, and the results can be seen in Figure 22. The time parameters are presented in Table 1. The decay was constantly 4 ns and not affected by the addition of DBU. However, the time to obtain the same number of counts increased as the concentration of base increased. This indicates some static quenching processes are transpiring when the base was added and nonradiative processes are becoming more dominant without changing the rate of fluorescence. Moreover, when the absorption was not affected by the TCSPC measurements.

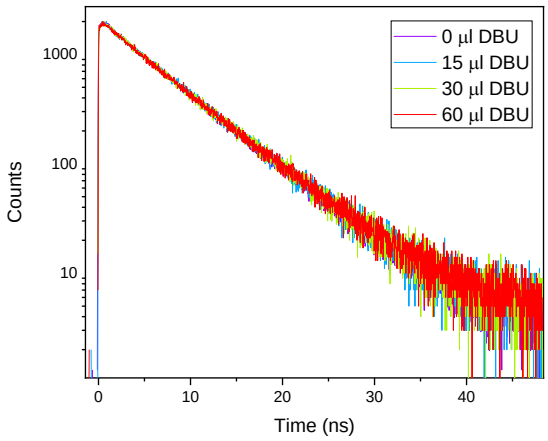

Figure 22 *Decay traces of PCA in acetonitrile with the addition of DBU collected with TCSPC at emission wavelength 600 nm.*

TA measurements were performed to investigate the deprotonation of PCA. In Figure 23 the decay of PCA with TBAOH is presented. As reference a decay of only PCA is also included, observe that the scales are different. It can be detected that the signal of the deprotonated PCA was decreased, similar to the result from the steady-state absorption and emission. The band at 200-300 nm is depleted, the peak at 457 nm has shifted to 440 nm. Additionally, the shape of the peak is changed upon addition of base. It could result from increased vibrational resolution upon deprotonated, however this could not be observed in the steady-state measurements. The TCSPC results suggested more non-radiative decay after deprotonation of PCA. Thus, new non-radiative states could be accessible, no positive features were detected. However, it is possible that there are some ESA overlapping with the stimulated emission peak around 400- 500 nm. By comparing the rates of decay at different wavelengths this hypothesis could be strengthened as the rate differentiate, at 424 nm is 7.2 ns while at 500 nm it is 7.0 ns, see Table 1 for time parameters. However, the sensitivity is low and no final conclusions could be drawn based on these values.

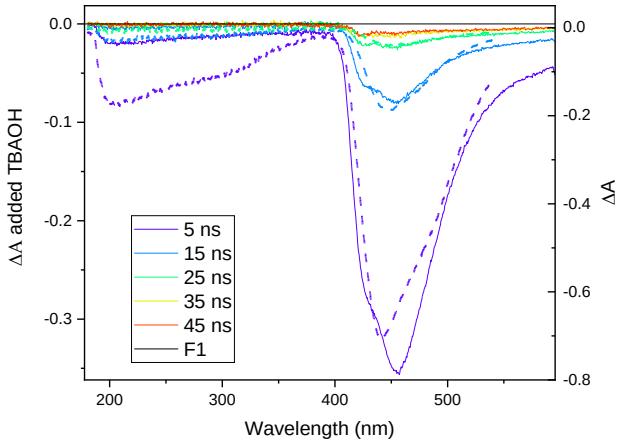

Figure 23 *TA measurement of PCA in acetonitrile with added TBAOH, the dashed lines are TA for PCA without base as a reference. The reference data is normalized to the first.*

In summary of the deprotonation effects on the chromophores; deprotonation of ACA leads to large shifts in absorption and emission, quenching the fluorescence and emission lifetime from 11 ns to <1 ns. For PCA deprotonation has ha smaller effect, no shifts are observed, and the emission lifetime is constant. However, new nonradiative process seems to occur, and the ΔA signal is decreased and peak shapes are changed in TA. Moving on, we will see how the photochemistry is further changed by addition of cations.

4.3 Cation interaction

The following sections will focus on ion-ion interactions and how the photophysical properties changes upon addition of sulphate salts. Shifts in absorption or emission peaks indicates shifts in the available energy states, hence, new interactions are occurring that changes the photochemistry. Changes in the detected photophysical signals from the chromophores upon addition of cations indicates complexation. Formation of a complex is the first step of studying SF with dynamic ion-ion bridges. A strong base was first added to the chromophore, before any sulphate salts, as we want to investigate only the ion-chromophore interaction and not the deprotonation. Similarly to the previously sections, the results regarding ACA will be presented first, followed by the addition to PCA. Modelling and a further discussion about complex formation will be presented in section 4.5.

4.3.1 Cation titration to ACA

Since ACA was used as a model system in the project, a more complete investigation of ion interactions with ACA was performed. The effects on the absorption and emission spectra additions of sulphate salts to ACA will first be presented. Followed with a discussion about the different interactions for different salts.

4.3.1.1 Effects on the absorption and emission spectrum

Different sulphate salts were added to DMSO solutions containing ACA, which had been deprotonated by DBU. The emission spectra and absorption spectra for the different additions can be observed in Supporting Information S.8. The normalized emission intensity at the wavelength 414 nm is plotted against the volume of salt solution added in Figure 24. Volume was used instead of molar ratio due to low solubility of some of the salts. The aimed concentration for all was 10 mM. Analysis of Figure 24 shows that the addition of $MnSO_4$, $CaSO_4$, and Na_2SO_4 did not

show any increase in emission intensity at 414 nm. In worst case, the salt did not dissolve at all, and the sample was just diluted from the additions. However, $MgSO_4$ had low solubility in DMSO and still an increase of emission intensity with a higher concentration can be observed.

The addition of $ZnSO_4$, $MgSO_4$, and $Al_2(SO_4)_3$ differentiate from the other salts. In Supporting Information S.8 isosbestic points can be observed of when Zn^{2+} and Mg^{2+} were added and the emission peaks are also slightly redshifted compared to deprotonated ACA. However, the peaks were still at shorter wavelengths than the emission of ACA without base. Hence, the addition of Zn^{2+} and Mg^{2+} seems to initiate a state in between deprotonated and neutral ACA. Ion-ion bonds are believed to be formed between the deprotonated ACA and Zn/Mg which can stabilize the anion, amplifying the steady-state emission intensity due to stabilization, and ACA could get more of its protonated photochemical properties.

Moreover, addition of Al^{3+} also increase the emission intensity, see Figure 24. Though, not from interaction of the cation and ACA^-, rather due to an increase at 465 nm which originates from the neutral ACA. Indicating that Al^{3+} interacts with the DBU leading to protonation of ACA rather than stabilizing the ACA, see Supporting information S.7 for emission and absorption spectra.

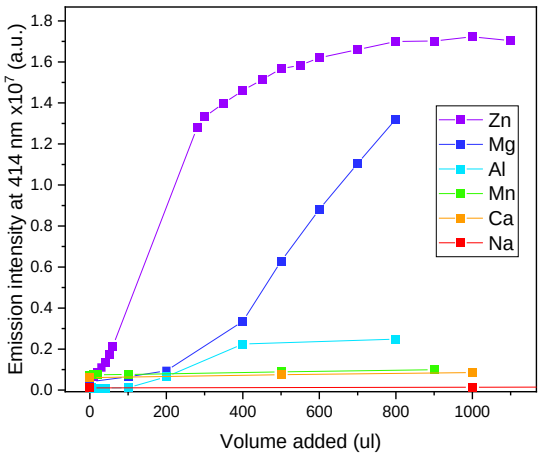

Figure 24 *Normalized emission intensity at 414 nm plotted against the volume of salt solution added to ACA with DBU in DMSO.*

4.3.1.2 Effect on emission lifetime

Attempting to confirm previous statements, emission lifetime measurements were performed. Addition of $ZnSO_4$ to ACA, with added DBU or added sulfuric acid were performed and TCSPC measurements at three different detection wavelengths between each step. The decay traces are presented in in Supporting Information S.9, and the time parameter obtained from monoexponential fitting over different volumes of $ZnSO_4$ added for the different conditions are presented in Figure 25. Acid was used to investigate the interaction between Zn^{2+} and ACA and not deprotonation of ACA by sulphate.

When acid was present the lifetime was constant, suggesting that there are no interactions between Zn^{2+} and neutral ACA. When $ZnSO_4$ was added to ACA the lifetime decreased from 11.7 ns to 8 ns, see Table 1. This change is assigned to deprotonation of ACA by sulphate followed by interaction of Zn^{2+} and ACA^-. Additions of $ZnSO_4$ to ACA deprotonated by DBU show an increase in emission lifetime, after 400 µl been added the same lifetimes are obtained as without addition

of DBU. This could imply that a 1:1 complex is formed at the end point, where complexes of higher orders are achieved at earlier additions. The complex formation will be further discussed in Section 4.5.

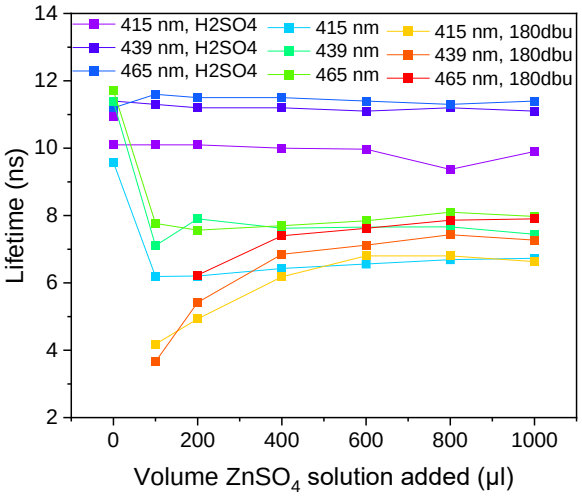

Figure 25 *Lifetime measurements for addition of $ZnSO_4$ to ACA in DMSO in different conditions. Three samples; H_2SO_4 +ACA, ACA, DBU + ACA. Excitation wavelength 377 nm, emission detected at 415, 439 and 465 nm.*

Additions of $MgSO_4$ to deprotonated ACA shows similar results as addition of $ZnSO_4$ in the sense that the emission lifetime was increased when $MgSO_4$ was added, see Figure 26. However, clearly new species are formed as two different slopes can be seen. Indicating that a more long-lived species was created and increased in concentration. Therefore, a bi-exponential equation was fitted to the decays. The time parameters, and the influence of the first preexponential factor A_1 is presented in Figure 26b. It can be observed that the second time parameter was increased in both value and influence as the concentration of $MgSO_4$ increased. A possible interaction with ACA^- and Mg^{2+} may lead to a more stable excited state and hence longer lifetimes. Perhaps a complex forming (i) stabilizes the excited state and/or (ii) enable access to new energy states.

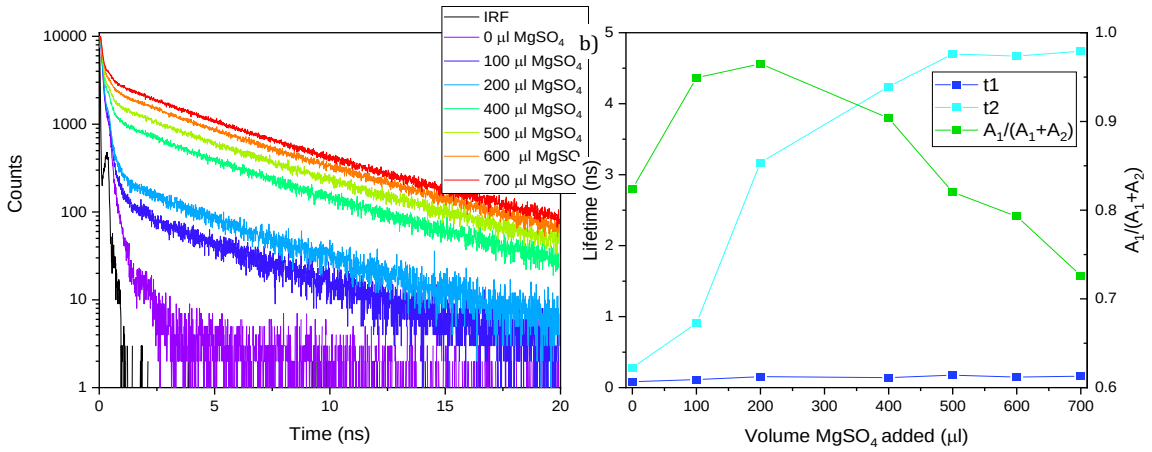

Figure 26 *Addition of 0-700 µl of MgSO4 to ACA with DBU in DMSO, a) TCSPC traces, emission detected at 465 nm b) time parameters (blue lines) and influence of preexponential factor A1 (red line) over addition of MgSO4.*

Note, an increase in lifetime might indicate complex formation, however SF would lead to a decrease in emission lifetime as new competing decay pathways would be available. An excess of

Mg^{2+} would most likely lead to a 1:1 complex and no free deprotonated ACA, a monoexpoential decay would then be sufficient. An excess was not reached in this experiment, the concentration of $MgSO_4$ added was unknown as the solubility in DMSO was poor.

4.3.2 Cation titration to PCA

The interactions with PCA and the cations Mg^{2+} and Zn^{2+} were investigated as they showed the most promising results with ACA. Due to the small change in photoactivity upon deprotonation of PCA, generally only small alterations could be observed from additions of sulphate salts to PCA. The effects on absorption and emission from addition of $ZnSO_4$ to PCA with DBU are presented in Figure 27. Initially, DBU lowers the absorption and the emission intensity. Subsequent addition of $ZnSO_4$ increased the emission intensity, absorption showed a small increase at 275 nm and the S_2 band at 400 nm. Simultaneously the absorption was decreased at the S_1 band, and at 318 nm.

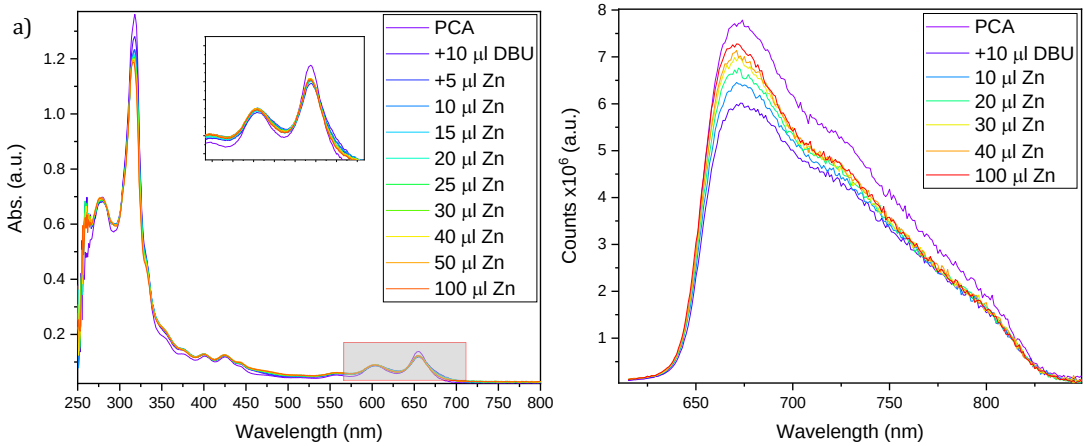

Figure 27 *Addition of $ZnSO_4$ to PCA in DMSO a) absorption spectrum b) emission, excitation wavelength 600 nm, slits 3 nm.*

Previously, an increase of emission intensity was explained as stabilization of the negative charge on the deprotonated chromophore by complex formation, and this description could still hold. A change in emission intensity could also originate from different decay pathways and how competitive they are. SF would be indicated if quenching could be detected, which not is the case here. However, a complex formation is thought to a necessary step before SF can occur on these low concentrations of PCA, and an increase in emission intensity could be a signal of stabilization through complexation. Careful TCSPC measurements or ultrafast TA might give some more insight on what is happening in the system.

The excitation and emission spectrum of addition of $MgSO_4$ to PCA with DBU in acetonitrile is presented in Figure 28. As $MgSO_4$ is added the emission intensity was decreased, thus, nonradiative processes may be increasing. Supporting the hypothesis that Mg-PCA complexes are formed and facilitate SF. However, the decrease may also be due to light scattering due to the low solubility of $MgSO_4$ in acetonitrile. The low concentration of PCA and light scattering from not fully dissolved $MgSO_4$ made the absorption spectrum hard to interpret. A redshift can also be observed for both the emission and excitation spectra.

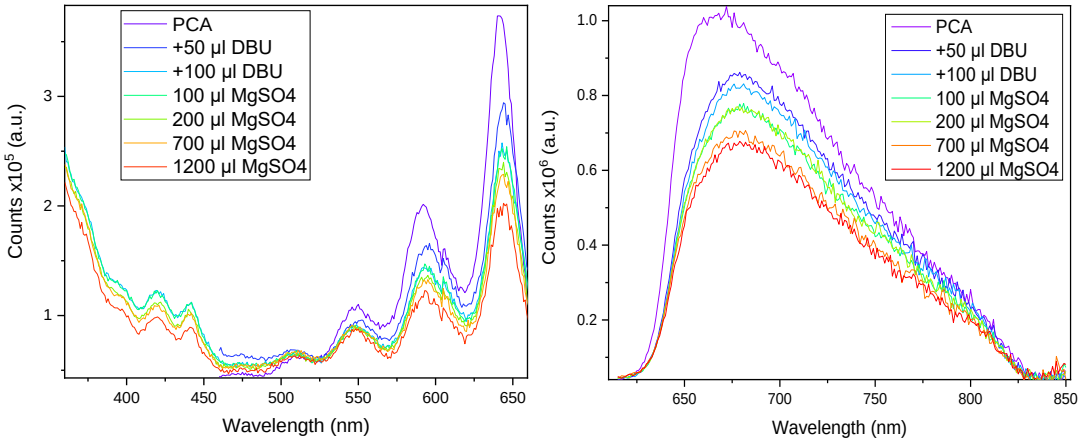

Figure 28 *Addition of MgSO4 to PCA in acetonitrile, a) excitation spectra at 673 nm entrance and exit split 4 nm b) emission spectra excitation wavelength 600 nm, entrance and exit split 3 nm.*

4.4 Decay rates

Evaluating the decay rates for different states and how they are affected by deprotonation and ion-ion interactions may give insights about the processes occurring in the system. TCSPC have been used to determine the emission lifetime by fitting the obtained data to a mono- or biexponential decay, see Equation 10. Moreover, the decays measured with TA at some selected wavelengths have also been fitted to the same monoexponentional equation. The obtained parameters are presented in Table 1. In some cases, fitting to a biexponential equation was considered necessary, and those parameters are therefore included.

Table 1 *Results from exponential fitting from decays obtained by TCSPC (or TA which are noted with an asterisk)*

Excitation wavelength	Sample	Detection wavelength	A1	t1	A2	t2	R-Square (COD)
415*	ACA-221103	210	-0.08	11.02			0.956
		406	-1.19	16.51			0.998
		445	-1.42	21.9			0.992
		530	-0.76	13.80			0.999
		870	-0.11	12.52			0.996
	ACA-221110	406	-0.520	14.9			0.998
		445	-0.94	17.6			0.995
		509	-0.46	14.5			0.998
	ACA with Zn excess-221110	210	-0.03	9.00			0.784
		409	-1.18	12.03			0.995
		530	-0.18	10.18			0.997
		870	-0.14	9.03			0.996
		415	7.54E+03	9.58			0.986
		439	9.86E+03	11.40			0.999
		465	1.04E+04	11.70			1.000
377	ACA	465	9.92E+02	11.68			0.997
		465	7.43E+02	11.71			0.995
	ACA+60 µl DBU	465	7.43E+02	11.71			1.46E+02
	ACA+120 µl DBU	465	1.82E+03	0.16	1.61E+02	11.62	4.21E+01

	ACA+180 µl DBU	465	2.28E+03	0.17			4.00E+01
	ACA+Zn	415	7.81E+03	6.73			0.992
		439	9.62E+03	7.44			0.996
		465	1.01E+04	7.97			0.998
		465	1.82E+03	0.16	1.61E+02	11.62	0.986
		439	1.09E+04	0.23	2.74E+02	1.00	
	ACA+DBU+Zn	415	9.16E+04	0.98	9.65E+03	7.46	0.999
		439	8.63E+04	0.98	1.20E+04	7.95	0.999
		465	3.49E+05	0.68	1.32E+04	8.17	0.999
	ACA+DBU+Mg	465	5.98E+03	0.25	1.23E+03	4.37	0.994
	ACA+DBU+Mn	456	1.73E+04	0.22	3.52E+01	2.46	0.997
	ACA+DBU+Na	465	2.96E+04	0.07	8.42E+03	0.24	0.998
	ACA+DBU+Al	465	9.48E+03	10.79			
	ACA+DBU+Ca	465	5.83E+04	0.20	1.93E+03	1.00	
415*	PCA	206	-0.51	5.22			0.998
		432	-0.30	5.33			0.997
		446	-3.01	7.70			0.996
		647	-0.09	7.93			0.993
600*		205	-0.05	6.30			0.984
		288	-0.09	5.90			0.993
		647	-0.13	6.01			0.995
		757	-0.17	5.68			0.998
		667	-0.30	6.29			0.999
	PCA+ TBAOH	206	-0.046	6.19			0.965
		424	-0.51	7.24			0.993
		455	-0.73	6.90			0.997
		500	-0.36	6.96			0.995
560	PCA (acetonitile)	432	1.12E+04	4.10			0.999
		673	2.18E+03	6.13			0.999
		670	5.18E+02	0.81	4.34E+03	3.54	0.999
	PCA+Zn	432	4.98E+03	2.07			0.999
		670	2.33E+02	1.21	7.99E+02	3.72	0.998
	PCA+DBU	673	2.09E+03	6.31			0.998
	PCA+ DBU +Zn	432	2.62E+03	0.90	7.70E+03	4.17	1.000

Let's first consider the rates regarding neutral ACA. The peak at 445 nm in TA was previously assigned to originate from emission. However, there is a 20 nm shift compared to the steady-state emission, detected at 465 nm, and the peak decay rate variates from 21.9 ns to 17.6 ns and 11.7 ns respectively. The peak detected at 445 in TA could therefore not be originating from emission. There may also be a dependency of excitation wavelength as 377 nm and 415 were used respectively. To rule this out a steady-state emission measurement where 415 nm is used an excitation wavelength could be conducted.

However, the rates from TA also show alterations, see Figure S.15 in Supporting information S.9. The measurements of ACA decay at the peak wavelength for TA and TCSPC is presented in **Figure**

29 over time. It can be concluded that the rates differentiate, even between the two TA measurements with the same concentration. Therefore, the system might have a power dependency as the laser power may shift during the day and from day to day. That could indicate a pseudo first order decay where a molecule in the GS quenches the excited state. Higher power would lead to a higher ΔA value, and fewer molecules are left in GS. Therefore, the lifetime would increase as the probability of a molecule in the excited state meeting a molecule in the ground state decreases. That could also explain the shorter lifetime for the TCSPC measurements as the diode has lower power than the pulsed laser used in TA. Nevertheless, these are only speculations and power dependency measurements would be necessary before any certain conclusions can be drawn.

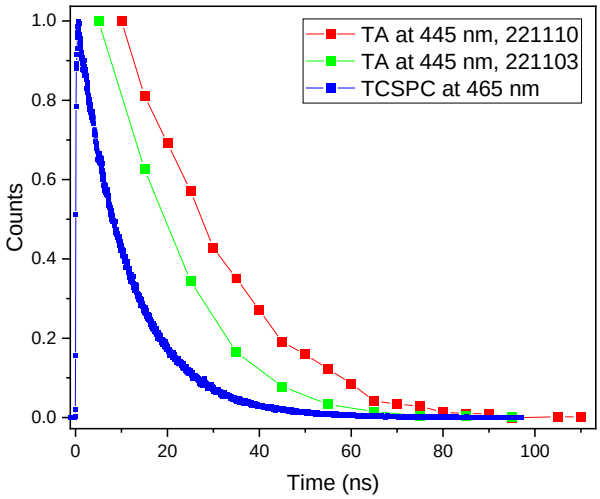

Figure 29 *Normalized decay of ACA in DMSO measured with TA at two different occasions and with TCSPC respectively.*

Deprotonation decreases the emission lifetime of ACA drastically to <1 ns. When cations are added, a biexponential fitting becomes necessary, as there now both are free deprotonated chromophores and chromophores that interacts with cations. For Zn^{2+} and Mg^{2+} the secondary time parameter increases in influence and are 8. 2 ns and 4.2 ns respectively.

The lifetime of PCA is roughly 4 ns in all measurements TCSPC, independently on deprotonation and cation addition. Measured with TA the lifetime is around 6 ns. This supports the previously discussion about the results from steady-state, the photochemistry of PCA is little affected by deprotonation and ion-ion interactions.

Noteworthy, the sensitivity of the fittings from TA measurements should be considered low. Few data points are available, and the CCD camera was used a detector. For more accurate lifetimes, the PMT detector should be utilized.

4.5 Complex formation

The previous section 4.3 showed that there are indication of ion and chromophore interaction where the photochemistry seems to be affected by the addition of cations. Possible complex formation between the chromophores is important to investigate to see if it results in chromophores being in confined and defined positions relative each other. The probability for SF at lower concentrations is believed to be increased as well as decrease the chance for TTA or other loss pathways if complexes can be formed. The interaction of ACA and Zn^{2+} were selected to be

further investigated through modulation of the Benesi-Hildebrand method and ITC measurements.

The properties of the system were previously unknown, assumptions are thus necessary. The hypothesis suggests the chromophores are close together during excitation and propagation followed by dissociation before recombination of the excited states can occur. The complex formed should therefore be of a higher order than one and at least the second binding should be reversible.

Several equilibriums need to be considered for the titration of Zn^{2+} to ACA, see R2, R3, and R4.

$$Zn^{2+} + ACA^- \underset{k_1'}{\overset{k_1}{\rightleftarrows}} (\mathrm{ZnACA})^+ \quad (R2)$$

$$(\mathrm{ZnACA})^+ + ACA^- \underset{k_2'}{\overset{k_2}{\rightleftarrows}} \mathrm{ZnACA_2} \quad (R3)$$

$$\mathrm{ZnACA_2} + Zn^{2+} \underset{k_3'}{\overset{k_3}{\rightleftarrows}} 2(\mathrm{ZnACA})^+ \quad (R4)$$

The equilibrium constants are presented in Equation 14 where k_1 is for the first binding event, k_2 is for the second, and k_3 for the formation of a 1:1 complex from a 2:1. The equilibrium constants for the equilibriums can be described as in Equation 14.

$$K_1 = \frac{[(ZnACA)^+]}{[Zn^{2+}][ACA^-]} = \frac{k_1}{k_1'} \quad K_2 = \frac{[(ZnACA_2)]}{[(ZnACA)^+][ACA^-]} = \frac{k_2}{k_2'} \quad K_3 = \frac{[(ZnACA)]^+}{[(ZnACA_2)][Zn^{2+}]} = \frac{k_3}{k_3'} \quad (14)$$

4.5.1 Benesi-Hildebrand modelling

To examine the binding events the Benesi Hildebrand method (BH) was used. The traditional BH only accounts for a 1:1 complex, hence the method needs to be modified. There are several different approaches and attempts previously made to model a 1:2 complex. However, many assumptions have been made for them to work. Therefore, they cannot be used directly in our case. Moreover, the absorption comes from the chromophores that are the ligands in the complex, therefore Zn^{2+} was added to ACA^-. In other words, the host was added to the guest, which normally not is the case.

At the end of the titration Zn^{2+} was in excess, a 1:1 complex can be a predicted rather than a complex of a higher order. A 2:1 complex can instead be expected when ACA is in excess which is the case in the first additions of Zn. Therefore, very small steps of Zn at a low concentration were necessary to be able to see any of the presence of $\mathrm{ZnACA_2}$. Two titrations were made, one with lager steps where Zn was added until excess was reached and one where only small additions of Zn were added, the absorption was measured between each addition. The absorption spectra for the former can be observed in Figure 30.

It can be observed in Figure 30b that the rate of change in absorption changes over the titration. The absorption changes only a little in the initial additions, to then have a drastic change and finally change very little. This indicates that there are multiple processes occurring simultaneously. Three different approaches have been attempted to define what was happening, full derivations of the models are presented in Supporting Information S.2.

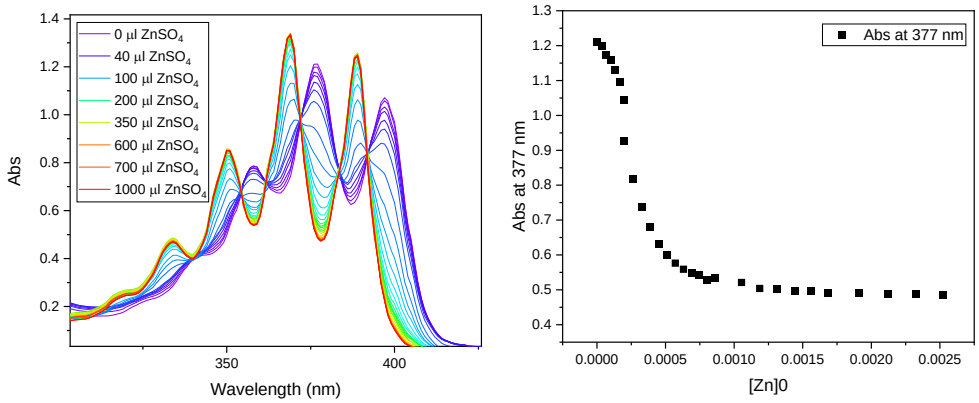

Figure 30 *Titration of ZnSO4 to ACA fully deprotonated with DBU, a) Absorption spectra, b) absorption at wavelength 377 nm versus concentration of Zn.*

Firstly, a 1:1 complex was assumed; all ACA would be part of a complex when Zn^{2+} was in excess. The concentration of the complex could then be calculated according to the Benesi-Hildebrand equation presented in Equation 8. The concentration $[Zn^{2+}]$, $[ACA^{-}]$, and $[ZnACA^{+}]$ were plotted versus the number of steps of added $ZnSO_4$, see Supporting Information S.2.1. The model gave negative concentration of Zn^{2+}, hence is not physical possible and the model can be discarded.

Secondly, a 1:2 complex was considered with irreversible binding. Again, a graphical analysis was performed, see Supporting Information S.2.2. The concentration of the complex was estimated to be higher than the total concentration of Zn added, which is unreasonable. Thus, the model showcases that an irreversible 1:2 complex cannot be possible.

Therefore, a third equilibrium must be taken into consideration, where the addition of Zn leads to dissociation from the 1:2 complex and instead form a 1:1 complex, see R4.

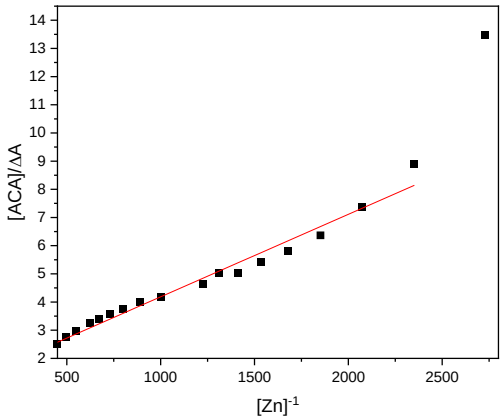

Figure 31 *Benesi-Hildebrand plot for the formation of a 1:1 complex from a 1:2 complex.*

The concentration of ACA divided by the delta absorption was plotted against $1/[Zn^{2+}]$, aa linear regression was made for the last part of the titration, see Figure 31. A value of an observed binding constant, K_{obs}, and molar excitation coefficient of the complexes, $\varepsilon_{complex}$, could be determined to be, 2.7E8 and 796 $cm^{-1}M^{-1}$ respectively. These are similar values obtained from a previous attempt

to iterate the values. Nevertheless, the fitting presented in Figure 31 is not perfect which should be taken into consideration when evaluating the determined values.

The observed binding constant should be a value of the ration between the two real bindings constants, these cannot be determined without iteration and thoughtful modelling which is outside of the scope of this thesis. It should be noted that even if the system at first glance can seem quite simple, two following reversible binding events, modelling it can quickly become complicated.

4.5.2 Isothermal titration calorimetry measurements

To study the events and promote the formation of the second complex, ACA was added to Zn and analyzed by ITC. A matrix of different addition combinations was carried out (ACA into DMSO,

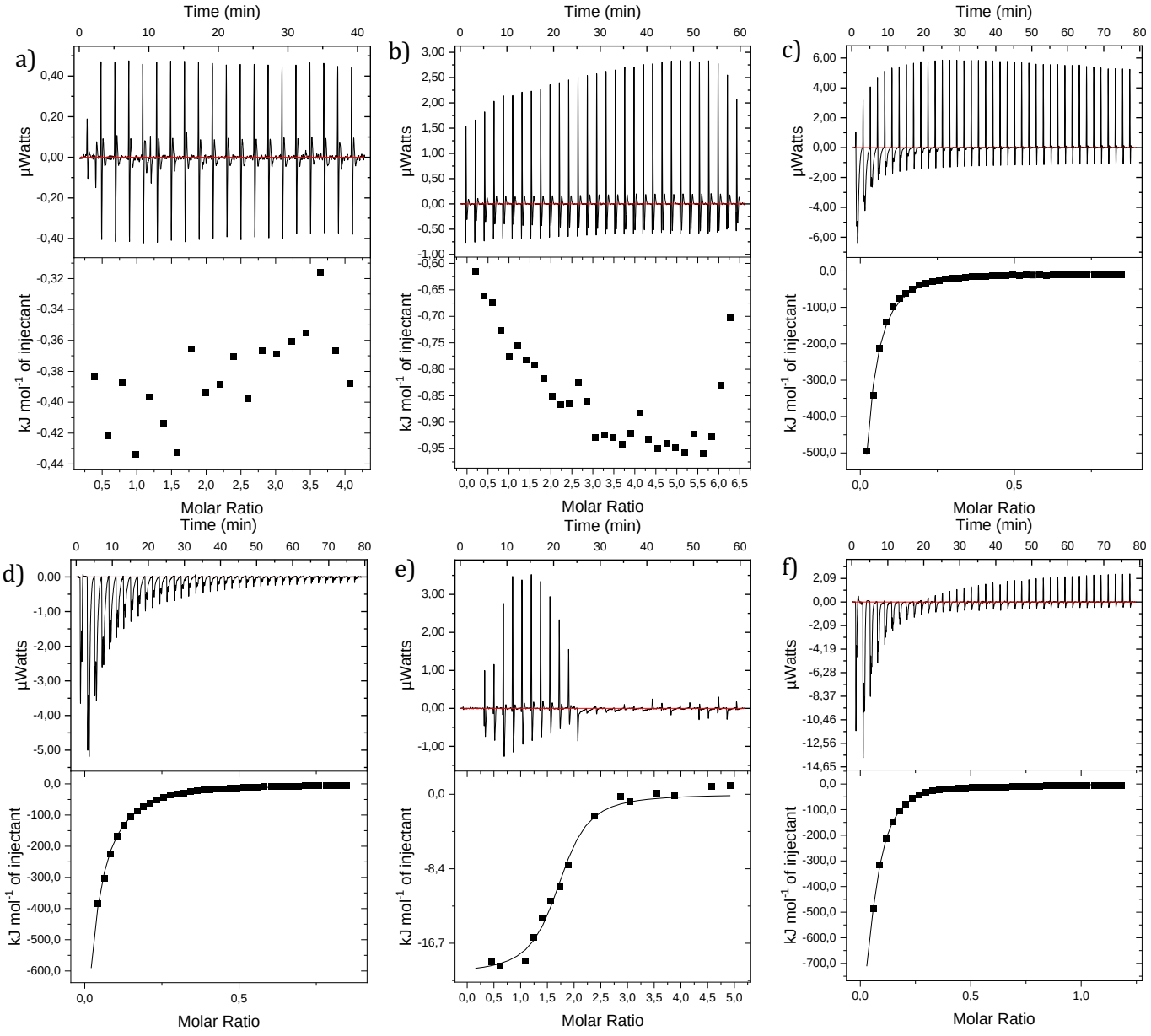

Figure 32 *Results from ITC measurements. thermograph (above) and Wiseman plot (below) against molar ratio. From left to right a) DMSO into DMSO. b) ACA into DMSO c) ACA with DBU into DMSO d) DBU into DMSO e) ACA into ZnSO4 in DMSO f) ACA with DBU into ZnSO4 in DMSO.*

ACA with DBU into DMSO, DBU into DMSO, ACA into $ZnSO_4$, ACA with DBU into $ZnSO_4$), the thermographs and Wiseman plots can be observed in Figure 32. Positive features in the thermographs can be observed in all were combinations except DBU into DMSO, and it seems to be much fluctuation in the data. This is probably caused by instrumental insensitivity as it was calibrated for aqueous solutions and not DMOS. The heat capacity of DMSO is 0.47 cal g^{-1} K^{-1} while water per definition has 1 cal g^{-1} K^{-1}. Hence, too much heat was added when return to equilibrium was attempted. Different settings were tested without being able to remove these features.

Moreover, in the experiments when DBU was part of the mix, a large ΔH was observed around -400kJ/mol. This is thought to be deprotonation of water that possible still can left in the cell or not using dry enough DMSO. This is quite problematic since the binding of the ACA^- and Zn^{2+} cannot be detected when other processes with much large ΔH is occurring simultaneously. In Figure 32e ACA without DBU was added to $ZnSO_4$, then a ΔH of -16 kJ/mol was obtained instead and a molar ratio could be derived to be around two. However, the reproducibility has proven to be low as upon repeating the experiment similar results have not been achieved. Again, only the negative peaks were integrated which lowers the accuracy. It is possible that one of the biding events are endothermic which now would be totally neglected. Only a one site fitting could be used to gain a good fit, even though two sites were expected. From the shape of the Wisemans plot, only one inclination point can be observed indicating only one binding but there could be something hidden due to low sensitivity as previously mentioned.

4.6 Ultrafast transient absorption

The addition of Zn to PCA and ACA was studied using ultrafast transient absorption. The hope was to observe a change in propagation for a low concentration of the chromophore with and without zinc. A change that hopefully could indicate SF, would be an increase in triplet formation and a faster decay in signals coming from the singlet. Hence, there would now be additional processes quenching available for the singlet as undergo SF. Some preliminary experiments have been performed without an extended data analysis yet. Some change was observed between the different samples, but its origin has not been detected. The setup used for collecting the data is complicated with several sources or error, resulting in difficulties to interpret if the features observed are real or not. More repetitions with smaller steps of addition of base and cation needs to be performed until something can be said with certainty if ion-ion interactions affect the ability of SF.

4.7 Future work

The result presented within this thesis has focused on the characterization of the chromophores ACA and PCA and how deprotonation and interaction with cations affect their photochemistry and properties. However, the main goal is to investigate if ion-ion interactions can affect the probability of SF and from that learn more about the prerequisites and mechanisms for SF. Therefore, more accurate and elaborate fsTA measurements are necessary as a next step for understanding the properties better. The work at nsTA has given us an indication that something may occur, but to know what and on which time scale higher transient resolution is needed. Areas of investigation would then be; the progression of the excited states and if ion-ion interactions affect the electronic transitions.

Deprotonation of the carboxylic acids seems to change the photochemistry of the chromophores, for ACA much more pronounced changes than for PCA. This may be a good thing, not altering the energy levels too much for PCA. Nevertheless, the deprotonation is more difficult to detect. Thus,

having the carboxylic acid on one of the ends of the chromophore, and in this case with a phenyl group between can lead to less control of the orientation and distance of the chromophores related to each other. As previously mentioned, for SF to occur the distance and position of the two chromophores are important. Hence, the aim of making complexes with them. The position of the carboxylic acid could therefore have a great impact on the formation and shape of the complex. It would therefore be interesting to synthesize other pentacene carboxylic acids where the position of the acid is changed and then investigate the change in photochemistry upon deprotonation and addition of cations. Anchoring it at a position on the acene rings is predicted to give a large influence on the energy levels and a more confined complex structure.

Through BH modeling and analysis of the absorption and emission spectrum complexes of chromophores and ions seems to be present. Still, the orientation or the interactions between the chromophores has not been thoroughly studied. Again, this could have a large impact if SF can occur or not. The technique of fluorescence anisotropy may give some insight, where potential energy transfer could be detected.

The interaction between ACA and Zn has been more carefully investigated since the concentration could be decided due to good enough solubility. The binding coefficients and rates of the systems ACA-Mg, PCA-Mg, or PCA-Zn have however not been calculated. They could provide important information about the properties of the complexes such as the order and dissociation rate. Moreover, they may give insight into which conformation gives which photophysical properties that herein have been measured for different molar ratios without knowing with a high certainty which and if a complex has been formed.

Solubility has proven to be a rather big issue, where it has been troublesome to find a suitable solvent for both salts and chromophores. However, of course, not all solvents nor salts have been tested. Perhaps a good first approach would be to change the counter ion to, for example, chloride that is highly soluble in water, easily accessible, and is not predicted to interact further with the system.

SF has not yet been proven to occur in our system, for that to happen further fsTA measurements need to be performed. Other combinations and concentrations of chromophore, base, and cations are essential to study before any definite answer can be given regarding if ion-ion interactions can facilitate SF.

5. Conclusions

Several different techniques have been used to successfully characterize the photophysics of the chromophores ACA and PCA, the effect of deprotonation and ion-ion interactions. A satisfactory foundation for a potential continuation of the project have been laid, where knowledge about several important properties have been discovered. Such as the emission lifetimes, effect on photochemistry by deprotonation, ion-ion interactions, and complex formation. The result and discussion of this thesis, together with a small outlook, will herein be summarized.

ACA absorbs in the UV-region with the first peak at 386 nm. The emission spectrum is broad with a peak at 465 nm. The emission lifetime is of 11.7 ns. When ACA is deprotonated the absorption redshifts with 10 nm, the emission quenches and is blueshifted, the emission lifetime is reduced to >1 ns. Addition of $ZnSO_4$ to ACA give similar results as with deprotonation, but not as large changes. If $ZnSO_4$ is added to already deprotonated ACA a blueshift in absorption and a redshift in emission can be observed instead. Hence, a stabilization of the deprotonated state seems to occur. The emission lifetime is 4 ns after addition of $ZnSO_4$. Similar results were observed for the addition of $MgSO_4$. Addition of $MnSO_4$, $CaSO_4$, and Na_2SO_4 showed no changed. Addition of $Al_2(SO_4)_3$ interacts with the base resulting in an increase of the acid form of ACA.

PCA shows several different transitions band in absorption and do not submit to Kasha's rule as emission from two different states were observed upon excitation at 377 nm and 600 nm respectively. The emission lifetime was determined to be 6.2 ns. When base is added the absorption shows small change, the emission is quenched. When $ZnSO_4$ and $MgSO_4$ was added to deprotonated PCA an increase in emission could be observed indicating on interactions between the cations and the chromophore. Moreover, PCA has low light stability but is relative stable in solution.

Chromophore-ion complexes has been shown to form; the ion interactions are changing the photochemistry of the chromophores. A 2:1 complex is most likely formed of Zn:ACA and has been modulated with a modified Benesi-Hildebrand model and ITC measurements. Moreover, energy levels may possibly be tuned by ion interactions or degree of deprotonation which could lead to several valuable further implementations.

No ESA could be detected for ACA or PCA on their own, triplet sensitizations were done where PtOEP was added, a new long-lived feature of ACA could then be observed. A substantial ground state bleach arose. This information can later be used in the analysis of ultrafast transient absorption measurements that are the next neutral step of the project.

Singlet fission has not been proven to work in the proposed system, however, that would require more time than available within this project. Measurements within this report cannot say anything definite yet. No quenching observed in steady-state emission when ions are added, but more non-radiative possess seems to occur when analyzing the results from TCSPC.

Lastly, this work may be a part on the path to understand the mechanisms of SF better and in the extension improve the efficiency of solar panels. Nevertheless, more research is to be done.

References

[1] IRENA, " Renewable Energy Statistics 2022," The International Renewable Energy Agency, Abu Dhabi, 2022.

[2] "Best Research-Cell Efficiency Chart." U.S Department of Energy, Office of Energy Efficiency and Renewable Energy. https://www.nrel.gov/pv/cell-efficiency.html (accessed 28 August, 2022).

[3] W. Shockley and H. J. Queisser, "Detailed Balance Limit of Efficiency of p-n Junction Solar Cells," *Journal of Applied Physics,* vol. 32, no. 3, pp. 510-519, 1961/03/01 1961, doi: 10.1063/1.1736034.

[4] M. C. Hanna and A. J. Nozik, "Solar conversion efficiency of photovoltaic and photoelectrolysis cells with carrier multiplication absorbers," *Journal of Applied Physics,* vol. 100, no. 7, p. 074510, 2006/10/01 2006, doi: 10.1063/1.2356795.

[5] E. Sundin *et al.*, "Singlet Fission and Electron Injection from the Triplet Excited State in Diphenylisobenzofuran–Semiconductor Assemblies: Effects of Solvent Polarity and Driving Force," *The Journal of Physical Chemistry C,* vol. 124, no. 38, pp. 20794-20805, 2020/09/24 2020, doi: 10.1021/acs.jpcc.0c06626.

[6] V. Gray, L. Weiss, and A. Rao, "Singlet Fission: Mechanisms and Molecular Design," in *Emerging Strategies to Reduce Transmission and Thermalization Losses in Solar Cells: Redefining the Limits of Solar Power Conversion Efficiency*, J. S. Lissau and M. Madsen Eds. Cham: Springer International Publishing, 2022, pp. 291-311.

[7] T. Wang, B.-Y. Zhang, and H.-L. Zhang, "Singlet Fission Materials for Photovoltaics: From Small Molecules to Macromolecules," *Macromolecular Rapid Communications,* https://doi.org/10.1002/marc.202200326 vol. 43, no. 16, p. 2200326, 2022/08/01 2022, doi: https://doi.org/10.1002/marc.202200326.

[8] N. V. Korovina *et al.*, "Singlet Fission in a Covalently Linked Cofacial Alkynyltetracene Dimer," *Journal of the American Chemical Society,* vol. 138, no. 2, pp. 617-627, 2016/01/20 2016, doi: 10.1021/jacs.5b10550.

[9] J. Li, H. Cao, Z. Zhang, S. Liu, and Y. Xia, "Research Progress on Singlet Fission in Acenes and Their Derivatives," *Photonics,* vol. 9, no. 10, p. 689, 2022. [Online]. Available: https://www.mdpi.com/2304-6732/9/10/689.

[10] J. Xia *et al.*, "Singlet Fission: Progress and Prospects in Solar Cells," *Advanced Materials,* https://doi.org/10.1002/adma.201601652 vol. 29, no. 20, p. 1601652, 2017/05/01 2017, doi: https://doi.org/10.1002/adma.201601652.

[11] A. J. Carrod, V. Gray, and K. Börjesson, "Recent advances in triplet–triplet annihilation upconversion and singlet fission, towards solar energy applications," *Energy & Environmental Science,* 10.1039/D2EE01600A vol. 15, no. 12, pp. 4982-5016, 2022, doi: 10.1039/D2EE01600A.

[12] B. Daiber, K. van den Hoven, M. H. Futscher, and B. Ehrler, "Realistic Efficiency Limits for Singlet-Fission Silicon Solar Cells," *ACS Energy Letters,* vol. 6, no. 8, pp. 2800-2808, 2021/08/13 2021, doi: 10.1021/acsenergylett.1c00972.

[13] H. Sakai, R. Inaya, N. V. Tkachenko, and T. Hasobe, "High-Yield Generation of Triplet Excited States by an Efficient Sequential Photoinduced Process from Energy Transfer to Singlet Fission in Pentacene-Modified CdSe/ZnS Quantum Dots," *Chemistry – A European Journal,* https://doi.org/10.1002/chem.201803257 vol. 24, no. 64, pp. 17062-17071, 2018/11/16 2018, doi: https://doi.org/10.1002/chem.201803257.

[14] K. R. Parenti *et al.*, "Bridge Resonance Effects in Singlet Fission," *The Journal of Physical Chemistry A,* vol. 124, no. 45, pp. 9392-9399, 2020/11/12 2020, doi: 10.1021/acs.jpca.0c08427.

[15] E. G. Fuemmeler *et al.*, "A Direct Mechanism of Ultrafast Intramolecular Singlet Fission in Pentacene Dimers," *ACS Central Science,* vol. 2, no. 5, pp. 316-324, 2016/05/25 2016, doi: 10.1021/acscentsci.6b00063.

[16] J. M. Hollas, *Modern spectroscopy, Fourth Edition*. West Sussex, England: Jhon Wiley & Sons Ltd, 2004.

[17] M. Kasha, "Characterization of electronic transitions in complex molecules," *Discussions of the Faraday Society,* 10.1039/DF9500900014 vol. 9, no. 0, pp. 14-19, 1950, doi: 10.1039/DF9500900014.
[18] J. R. Lakowicz, Ed. *Principles of Fluorescence Spectroscopy*, 3 ed. Springer New York, NY, 2006, p. 954.
[19] M. Toutounji, "A deeper look into Herzberg-Teller vibronic coupling effect and spectroscopic signature of non-Condon systems," *Chemical Physics,* vol. 523, pp. 205-210, 2019/07/01/ 2019, doi: https://doi.org/10.1016/j.chemphys.2019.04.008.
[20] S. Ito, T. Nagami, and M. Nakano, "Molecular design for efficient singlet fission," *Journal of Photochemistry and Photobiology C: Photochemistry Reviews,* vol. 34, pp. 85-120, 2018/03/01/ 2018, doi: https://doi.org/10.1016/j.jphotochemrev.2018.01.002.
[21] M. B. Smith and J. Michl, "Singlet Fission," *Chemical Reviews,* vol. 110, no. 11, pp. 6891-6936, 2010/11/10 2010, doi: 10.1021/cr1002613.
[22] N. Maity *et al.*, "Parallel triplet formation pathways in a singlet fission material," *Nature Communications,* vol. 13, no. 1, p. 5244, 2022/09/06 2022, doi: 10.1038/s41467-022-32844-6.
[23] S. Paul, C. Govind, and V. Karunakaran, "Planarity and Length of the Bridge Control Rate and Efficiency of Intramolecular Singlet Fission in Pentacene Dimers," *The Journal of Physical Chemistry B,* vol. 125, no. 1, pp. 231-239, 2021/01/14 2021, doi: 10.1021/acs.jpcb.0c08590.
[24] R. Ringström *et al.*, "Molecular rotational conformation controls the rate of singlet fission and triplet decay in pentacene dimers," *Chemical Science,* 10.1039/D1SC06285A vol. 13, no. 17, pp. 4944-4954, 2022, doi: 10.1039/D1SC06285A.
[25] K. R. Parenti, He, G., Sanders, S.N., Pun, A.B., Kumarasamy, E., Sfeir, M.Y., Campos, L.M., , "Bridge Resonance Effects in Singlet Fission," *The Journal of Physical Chemistry A,* vol. 124, pp. 9392–9399, 2020, doi: doi:10.1021/acs.jpca.0c08427.
[26] M. Chen, Y. J. Bae, C. M. Mauck, A. Mandal, R. M. Young, and M. R. Wasielewski, "Singlet Fission in Covalent Terrylenediimide Dimers: Probing the Nature of the Multiexciton State Using Femtosecond Mid-Infrared Spectroscopy," *Journal of the American Chemical Society,* vol. 140, no. 29, pp. 9184-9192, 2018/07/25 2018, doi: 10.1021/jacs.8b04830.
[27] A. Trummal, L. Lipping, I. Kaljurand, I. A. Koppel, and I. Leito, "Acidity of Strong Acids in Water and Dimethyl Sulfoxide," *The Journal of Physical Chemistry A,* vol. 120, no. 20, pp. 3663-3669, 2016/05/26 2016, doi: 10.1021/acs.jpca.6b02253.
[28] G. A. Harlow and D. B. Bruss, "Titration of Weak Acids in Nonaqueous Solvents. Potentiometric Studies in Inert Solvents," *Analytical Chemistry,* vol. 30, no. 11, pp. 1833-1836, 1958/11/01 1958, doi: 10.1021/ac60143a036.
[29] J. S. Fritz and N. M. Lisicki, "Titration of Acids in Nonaqueous Solvents," *Analytical Chemistry,* vol. 23, no. 4, pp. 589-591, 1951/04/15 1951, doi: 10.1021/ac60052a012.
[30] H. A. Benesi and J. H. Hildebrand, "A Spectrophotometric Investigation of the Interaction of Iodine with Aromatic Hydrocarbons," *Journal of the American Chemical Society,* vol. 71, no. 8, pp. 2703-2707, 1949/08/01 1949, doi: 10.1021/ja01176a030.
[31] W. M. Ward, B. H. Farnum, M. Siegler, and G. J. Meyer, "Chloride Ion-Pairing with Ru(II) Polypyridyl Compounds in Dichloromethane," *The Journal of Physical Chemistry A,* vol. 117, no. 36, pp. 8883-8894, 2013/09/12 2013, doi: 10.1021/jp404838z.
[32] K. A. Ahmad Masood, Ranjan Raushan "Current Trends in Renewable Energy: An Overview," *International Journal of Engineering Research and Advanced Technology (IJERAT),* vol. 4, no. 5, 2018, doi: http://dx.doi.org/10.7324/IJERAT.2018.3257.
[33] "Chapter 7 - High Efficiency Plants and Building Integrated Renewable Energy Systems," in *Handbook of Energy Efficiency in Buildings*, F. Asdrubali and U. Desideri Eds.: Butterworth-Heinemann, 2019, pp. 441-595.
[34] V. V. Tyagi, N. A. A. Rahim, N. A. Rahim, and J. A. L. Selvaraj, "Progress in solar PV technology: Research and achievement," *Renewable and Sustainable Energy Reviews,* vol. 20, pp. 443-461, 2013/04/01/ 2013, doi: https://doi.org/10.1016/j.rser.2012.09.028.

[35] D. Yang, D. Yang, Ed. *Handbook of Photovoltaic Silicon*, 1 ed. Springer Berlin, Heidelberg, 2019, pp. XVIII, 967.

[36] C. Ramírez-Márquez and M. Martín, "Chapter 10 - Photovoltaic solar energy," in *Sustainable Design for Renewable Processes*, M. Martín Ed.: Elsevier, 2022, pp. 397-439.

[37] A. J. a. F. Bard, L.R., *Electrochemical Methods: Fundamentals and Applications. 2nd Edition*. New York: John Wiley & Sons, 2001.

[38] S. Kim, V. Q. Hoang, and C. W. Bark, "Silicon-Based Technologies for Flexible Photovoltaic (PV) Devices: From Basic Mechanism to Manufacturing Technologies," *Nanomaterials,* vol. 11, no. 11, p. 2944, 2021. [Online]. Available: https://www.mdpi.com/2079-4991/11/11/2944.

[39] T. Wang, B. Y. Zhang, and H. L. Zhang, "Singlet Fission Materials for Photovoltaics: From Small Molecules to Macromolecules," (in eng), *Macromol Rapid Commun,* vol. 43, no. 16, p. e2200326, Aug 2022, doi: 10.1002/marc.202200326.

[40] M. G. Hemeida, A. M. Hemeida, T. Senjyu, and D. Osheba, "Renewable Energy Resources Technologies and Life Cycle Assessment: Review," *Energies,* vol. 15, no. 24, p. 9417, 2022. [Online]. Available: https://www.mdpi.com/1996-1073/15/24/9417.

[41] "What is renewable energy?" https://www.un.org/en/climatechange/what-is-renewable-energy (accessed 14 November, 2022).

[42] M. Koese, C. F. Blanco, G. Breeman, and M. G. Vijver, "Towards a more resource-efficient solar future in the EU: An actor-centered approach," *Environmental Innovation and Societal Transitions,* vol. 45, pp. 36-51, 2022/12/01/ 2022, doi: https://doi.org/10.1016/j.eist.2022.09.001.

[43] O. O. Apeh, E. L. Meyer, and O. K. Overen, "Contributions of Solar Photovoltaic Systems to Environmental and Socioeconomic Aspects of National Development—A Review," *Energies,* vol. 15, no. 16, p. 5963, 2022. [Online]. Available: https://www.mdpi.com/1996-1073/15/16/5963.

[44] B. Huang *et al.*, "Life cycle cost analysis of solar energy via environmental externality monetization," *Science of The Total Environment,* vol. 856, p. 158910, 2023/01/15/ 2023, doi: https://doi.org/10.1016/j.scitotenv.2022.158910.

[45] R. Berera, R. van Grondelle, and J. T. M. Kennis, "Ultrafast transient absorption spectroscopy: principles and application to photosynthetic systems," *Photosynthesis Research,* vol. 101, no. 2, pp. 105-118, 2009/09/01 2009, doi: 10.1007/s11120-009-9454-y.

[46] F. Sha, T.-Y. Tai, M. A. Gaidimas, F. A. Son, and O. K. Farha, "Leveraging Isothermal Titration Calorimetry to Obtain Thermodynamic Insights into the Binding Behavior and Formation of Metal–Organic Frameworks," *Langmuir,* vol. 38, no. 22, pp. 6771-6779, 2022/06/07 2022, doi: 10.1021/acs.langmuir.2c00812.

[47] W. R. Archer and M. D. Schulz, "Isothermal titration calorimetry: practical approaches and current applications in soft matter," *Soft Matter,* 10.1039/D0SM01345E vol. 16, no. 38, pp. 8760-8774, 2020, doi: 10.1039/D0SM01345E.

[48] M. M. Pierce, C. S. Raman, and B. T. Nall, "Isothermal titration calorimetry of protein-protein interactions," (in eng), *Methods,* vol. 19, no. 2, pp. 213-21, Oct 1999, doi: 10.1006/meth.1999.0852.

[49] S. Satoshi, F. Tsuneo, Y. Nobuyuki, K. Shigeru, and I. Toshiko, "Absorption and Fluorescence Spectra of Anthracenecarboxylic Acids. I. 9-Anthroic Acid and Formation of Excimer," *Bulletin of the Chemical Society of Japan,* vol. 51, no. 9, pp. 2460-2466, 1978, doi: 10.1246/bcsj.51.2460.

[50] N. Ghoneim, D. Scherrer, and P. Suppan, "Dual luminescence, structure and excimers of 9-anthracene carboxylic acid," *Journal of Luminescence,* vol. 55, no. 5, pp. 271-275, 1993/08/01/ 1993, doi: https://doi.org/10.1016/0022-2313(93)90022-F.

[51] A. Maliakal, K. Raghavachari, H. Katz, E. Chandross, and T. Siegrist, "Photochemical Stability of Pentacene and a Substituted Pentacene in Solution and in Thin Films," *Chemistry of Materials,* vol. 16, no. 24, pp. 4980-4986, 2004/11/01 2004, doi: 10.1021/cm049060k.

[52] F. A. Schaberle *et al.*, "The Photophysical Properties of Triisopropylsilyl-ethynylpentacene—A Molecule with an Unusually Large Singlet-Triplet Energy Gap—In Solution and Solid Phases," *Chemistry,* vol. 2, no. 2, pp. 545-564, 2020. [Online]. Available: https://www.mdpi.com/2624-8549/2/2/33.

[53] N. V. Karimova, M. Luo, V. H. Grassian, and R. B. Gerber, "Absorption spectra of benzoic acid in water at different pH and in the presence of salts: insights from the integration of experimental data and theoretical cluster models," *Physical Chemistry Chemical Physics,* 10.1039/C9CP06728K vol. 22, no. 9, pp. 5046-5056, 2020, doi: 10.1039/C9CP06728K.

Supporting Information

S.1 Project overview

In Table S2 an overview of all the experiments conducted during the project are presented.

Table S2 *Overview of experiments conducted*

System			Measuring technique				
Chromophore	Base	Sulphate salts	Steady-state absorption	Steady-state Emission/ excitation	TCSPC	TA	ITC
ACA	No base		X	X	X	X	X
		$ZnSO_4$	X	X	X	X	X
		$MgSO_4$	X	X			
	TBAOH		X	X			
	DBU		X	X	X	X	X
		$(Al)_2(SO_4)_3$	X	X			
		$MgSO_4$	X	X	X		
		$MnSO_4$	X	X			
		$ZnSO_4$	X	X	X	X	X
		Na_2SO_4	X	X			
		K_2SO_4	X	X			
PCA	No base		X	X	X	X	
		$ZnSO_4$	X	X	X	X	
		$MgSO_4$	X	X	X		
	TBAOH		X	X	X	X	
	DBU		X	X			
		$MgSO_4$	X	X	X		
		$ZnSO_4$	X	X	X		

S.2 Benesi -Hildebrand method

Derivation of the Benesi-Hildebrand Analysis. The Benesi-Hildebrand method is based on the change in absorbance when a species goes from being free in the bulk to be part of a complex. Combination of basic mass balance and Lambert-Beers law a relation between the change in absorption and molar extinction coefficient can be created. Let's assume a complex formation with L, ligand, and M, a metal cation, see S.2.R1.

$$L + M \rightleftharpoons LM \qquad (S.2.R1)$$

The equilibrium constant, K_{eq}, for the reaction can be derived as in equation S.2.1

$$K_{eq} = \frac{[LM]}{[L][M]} = \frac{[LM]}{([L_0] - [LM])([M_0] - [LM])} \qquad (S.2.1)$$

where $[L_0]$ is the concentration of ligand added, and $[M_0]$ is the total concentration of metal ions. The concentration of the complex, $[LM]$, can be determined by rearranging S.2.1 and solving for a second-degree equation, see Equation S.1.2 and S.2.3.

$$[LM]^2 - [LM]\left([L_0] + [M_0] + \frac{1}{K_{eq}}\right) + [L_0][M_0] = 0 \qquad (S.2.2)$$

$$[LM] = \frac{1}{2} * \left([L_0] + [M_0] + \frac{1}{K_{eq}}\right) \pm \sqrt{\left(\frac{1}{2} * \left([L_0] + [M_0] + \frac{1}{K_{eq}}\right)\right)^2 - [L_0][M_0]} \qquad (S.2.3)$$

From Lambert Beers law:

$$A_L = [L]\varepsilon_L l \qquad A_{LM} = [LM]\varepsilon_{LM} l \qquad A_0 = [L_0]\varepsilon_L l$$

It is assumed that the cation by itself is not absorbing in the measured interval, hence the total absorbance detected, A_{tot}, is the sum of the absorbance from the free ligand, A_L, and the absorbance from the complex, A_{LM}. The change in absorbance can be calculated as in Equation S.2.4.

$$\begin{gathered}\Delta A = A_{tot} - A_0 = A_L + A_{LM} - A_0 = [L]\varepsilon_L l + [LM]\varepsilon_{LM} l - [L_0]\varepsilon_L = \\ [L]\varepsilon_L l + [LM]\varepsilon_{LM} l - ([L] + [LM])\varepsilon_L l = [LM](\varepsilon_{LM} - \varepsilon_L) l = [LM]\Delta\varepsilon l\end{gathered} \qquad (S.2.4)$$

S.2.1 1:1 complex formation

Let's assume a 1:1 complex. the equilibrium could then be presented as in (SI.2.R2)

$$ACA^- + Zn^{2+} \rightleftharpoons (\mathrm{ZnACA})^+ \qquad (SI.2.R2)$$

The equilibrium constant. K. can therefore be calculated as in Equation SI.2.5.

$$K = \frac{[(ZnACA)^+]}{[Zn][ACA]} = \frac{[(ZnACA)^+]}{([Zn]_0 - [(ZnACA)^+])([ACA]_0 - [(ZnACA)^+])} \qquad (SI.2.5)$$

where $[(ZnACA)^+]$ is the concentration of the complex, $[Zn]$ is the concentration of free zinc, $[Zn]_0$ the concentration of added zinc, $[ACA]$ is the concentration of free ACA, and $[ACA]_0$ the concentration of added ACA.

The total absorption, A_{obs}, is the sum of the absorption form free ACA and from the complex, which can be expended according to Lambert-Beers law and the mass balance, see Equation SI.2.6.

$$\begin{gathered}A_{obs} = A_{ACA} + A_{(ZnACA)^+} = [ACA]\varepsilon_{ACA} + [(ZnACA)^+]\varepsilon_{c1} = \\ = ([ACA]_0 - [(ZnACA)^+])\varepsilon_{ACA} + [(ZnACA)^+]\varepsilon_{c1}\end{gathered} \qquad (SI.2.6)$$

If the mass balance used in equation SI.2.5 is again used and the absorption of ACA in absence of complex is subtracted an expression where the difference in absorption is only dependent on the concentration of complex and the difference in molar excitation coefficient, see Equation SI.2.7.

$$\begin{gathered}\Delta A = A_{obs} - A_0 = A_{obs} - [ACA]_0\varepsilon_{ACA} = \\ = ([ACA]_0 - [(ZnACA)^+])\varepsilon_{ACA} + [(ZnACA)^+]\varepsilon_{c1} - [ACA]_0\varepsilon_{ACA} = \\ = [(ZnACA)^+](\varepsilon_{c1} - \varepsilon_{ACA})\end{gathered} \qquad (SI.2.7)$$

When enough zinc has been added, all ACA can be considered to be part of a complex; hence $[(ZnACA)^+]$= $[ACA]_0$, and $[ACA] = 0$. Hence the molar excitation coefficient for the complex, ε_{c1}, can be determined as in SI.2.8.

$$\frac{A_{end}}{[ACA]_{0.end}} + \varepsilon_{ACA} = \epsilon_{C1} \qquad (SI.2.8)$$

Substituting this value into SI.2.5 and SI.2.6 the equilibrium constant can be derived for the different addition steps. If the assumptions are valid the K value should not differentiate substantially between the additions. Moreover, SI.2.7 will give the concentration of the complex, this is potted against the volume of $ZnSO_4$ added in Figure S.1.

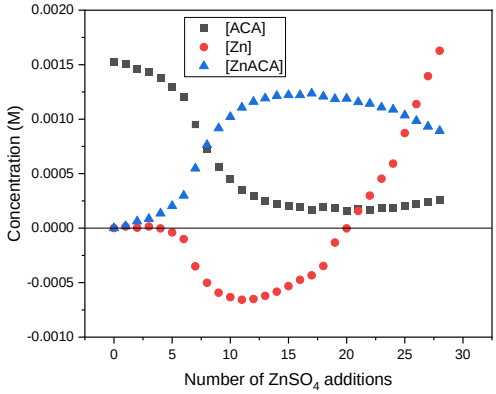

Figure S.1 *Concentration of free ACA, free Zn, and formed $(ZnACA)^+$ over the number of $ZnSO_4$ addition if a 1:1 complex with irreversible binding is assumed.*

S.2.2 1:2 complex with one binding event

If we instead assume a 1:2 complex forming but with only one binding event. or that the secondary binding event is so fast we can consider the 1:1 complex only as an intermediate. The equilibrium can be written as in SI.2.R3.

$$2ACA^- + Zn^{2+} \rightleftharpoons \mathrm{ZnACA_2} \qquad (SI.2.R3)$$

The equilibrium would hence be calculated as according to SI.2.9.

$$K = \frac{[ZnACA_2]}{[Zn][ACA]^2} = \frac{[ZnACA_2]}{([Zn]_0 - [ZnACA_2])([ACA]_0 - 2[ZnACA_2])^2} \qquad (SI.2.9)$$

The total absorption, A_{obs}, is the sum of the absorption form free ACA and from the complex, which can be expended according to Lambert-Beers law and the mass balance, see Equation SI.2.10.

$$\begin{aligned} A_{obs} = A_{ACA} + A_{ZnACa_2} = [ACA]\varepsilon_{ACA} + [\mathrm{ZnACA_2}]\varepsilon_{c2} = \\ = ([ACA]_0 - 2[\mathrm{ZnACA_2}])\varepsilon_{ACA} + [\mathrm{ZnACA_2}]\varepsilon_{c2} \end{aligned} \qquad (SI.2.10)$$

The difference in absorption can give an expression in terms of the concentration of the complex and the molar excitation coefficients, see SI.2.11.

$$\begin{aligned} \Delta A = A_{obs} - A_0 = A_{obs} - [ACA]_0\varepsilon_{ACA} = \\ = ([ACA]_0 - 2[\mathrm{ZnACA_2}])\varepsilon_{ACA} + [\mathrm{ZnACA_2}]\varepsilon_{c2} - [ACA]_0\varepsilon_{ACA} = \\ = [\mathrm{ZnACA_2}](\varepsilon_{c2} - 2\varepsilon_{ACA}) \end{aligned} \qquad (SI.2.11)$$

Again, at saturation, all ACA can be assumed to be in a complex, $[ZnACA_2]$= $[ACA]_0$. and $[ACA] = 0$. The molar extinction coefficient can be calculated as in Equation SI.2.12.

$$\frac{A_{end}}{[ACA]_{0.end}} + \varepsilon_{ACA} = \epsilon_{C2} \qquad (SI.2.12)$$

Substituting this value into SI.2.9 and SI.2.11 the equilibrium constant can be derived for the different addition steps. If the assumptions are valid the K value should not differentiate substantially between the additions.

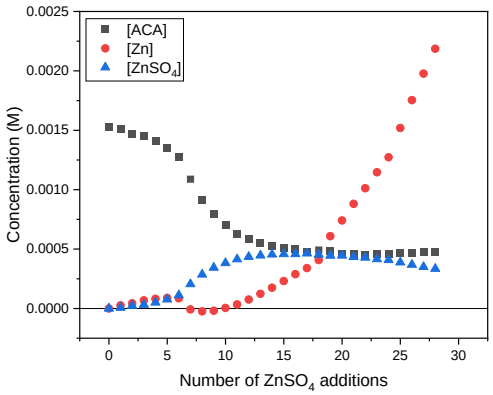

Figure S.2 Concentration of free ACA, free Zn, and formed $ZnACA_2$ over the number of $ZnSO_4$ addition if a 1:2 complex with irreversible binding is assumed.

S.2.3 1:2 complex with two reversible events

If instead a 1:2 complex is considered that can be formed by two irreversible reactions. see SI.2.R4 and SI.2.R5 for equilibrium reactions. At additional additions of Zn^{2+}, the main reaction would be the one presented in SI.2.R6.

$$Zn^{2+} + ACA^- \underset{k_1'}{\overset{k_1}{\rightleftarrows}} (\mathrm{ZnACA})^+ \qquad (SI.2.R4)$$

$$(\mathrm{ZnACA})^+ + ACA^- \underset{k_2'}{\overset{k_2}{\rightleftarrows}} \mathrm{ZnACA_2} \qquad (SI.2.R5)$$

$$\mathrm{ZnACA_2} + Zn^{2+} \rightleftarrows 2(\mathrm{ZnACA})^+ \qquad (SI.2.R6)$$

Now two equilibrium constants can be expressed as in SI.2.13 and SI.2.14.

$$K_1 = \frac{[(ZnACA)^+]}{[Zn][ACA]} = \frac{[(ZnACA)^+]}{([Zn]_0 - [(ZnACA)^+] - [ZnACA_2])([ACA]_0 - [(ZnACA)^+] - 2[ZnACA_2])} \qquad (SI.2.13)$$

$$K_2 = \frac{[\mathrm{ZnACA_2}]}{[(ZnACA)^+][ACA]} = \frac{[\mathrm{ZnACA_2}]}{[(ZnACA)^+]([ACA]_0 - [(ZnACA)^+] - 2[ZnACA_2])} \qquad (SI.2.14)$$

Moreover, the total absorbance can be expressed as in SI.2.15.

$$A = A_{ACA} + A_{(ZnACA)^+} + A_{ZnACa_2} =$$
$$= ([ACA]_0 - [(ZnACA)^+] - 2[\mathrm{ZnACA_2}])\varepsilon_{ACA} + [(ZnACA)^+]\varepsilon_{c1} + [\mathrm{ZnACA_2}]\varepsilon_{c2} \qquad (SI.2.15)$$

The difference in absorption can give an expression in terms of the concentrations of the complexes and the molar excitation coefficients. see SI.2.16.

$$\Delta A = A_{obs} - A_0 = A_{obs} - [ACA]_0\varepsilon_{ACA} =$$

$$= ([ACA]_0 - [(ZnACA)^+] - 2[\mathrm{ZnACA_2}])\varepsilon_{ACA} + [(ZnACA)^+]\varepsilon_{c1} + [\mathrm{ZnACA_2}]\varepsilon_{c2} - [ACA]_0\varepsilon_{ACA} =$$

$$= [(ZnACA)^+](\varepsilon_{c1} - \varepsilon_{ACA}) + [\mathrm{ZnACA_2}](\varepsilon_{c2} - 2\varepsilon_{ACA}) \quad (SI.2.16)$$

Now the same approach as before cannot be used where the saturation of zinc was used to calculate the molar excitation coefficients. Instead, the equilibrium presented SI.2.R6 needs to be used, where the observed bonding constant can be described as in Equation SI.2.17.

$$K_{obs} = \frac{[ZnACA^+]^2}{[ZnACA_2][Zn^{2+}]} \quad (SI.2.17)$$

By rearranging one can derived how the ΔA is related to the concentration of added guest, host and binding constant, see equation SI.2.18.

$$\Delta A = \frac{[ACA^-]K_{obs}[Zn^{2+}]}{1 + K_{obs}[Zn^{2+}]}\varepsilon_{complex} \quad (SI.2.18)$$

By rearranging this expression further, an expression like the one presented in SI.19 can be derived. where a linear regression to the measured data plots can be performed, where the intersect gives the $\varepsilon_{complex}$, and the slope gives the K_{obs}.

$$\frac{[ACA^-]}{\Delta A} = \frac{1}{\varepsilon_{complex}K_{obs}[Zn^{2+}]} + \frac{1}{\varepsilon_{complex}} \quad (SI.2.19)$$

S.3 Derivation of heat expression from ITC

The Gibbs free eneergy, ΔG, for a binidng event can be expressed in terms of R, the gas constant, T, the temperature, and the binding coefficient, K_a, see Equation SI.3.1.

$$\Delta G = RTln(K_a) \quad (SI.3.1)$$

Form the thermodynamics the free energy can also be expressed in terms of enthaply, ΔH, and entropy, ΔS, see Equarion SI.3.2.

$$\Delta G = \Delta H - T\Delta S \quad (SI.3.2)$$

Hence, the energy absorbed from an endothermic or relesed from an exothermic assoiciation event can be related to the heat evolved (Q), and the binding coefficient. Let θ be the fraction of sites on the metal (M) occupied by a ligand (L). It can be calculated as shown in Equation SI.3.3 where $[L]$ is the concentration of free ligand, and K_j iss the binding constant for binding event j.

$$\theta_j = \frac{[L]K_j}{1 + [L]K_j} \quad (SI.3.3)$$

The total ligand concentration $[L]_t$ is equal to the concentration of free ligand and the number of ligands in complexes, which can be expressed as in Equation SI.3.4.

$$[L_t] = [L] + M_t \sum_{j=1}^{k} (n_j\theta_j) \quad (SI.3.4)$$

The total heat produced can be described as the total conventration of hostes, multiplied with the fraction of sites that binds and the molar entalpy change, ΔH_j, see Equation SI.3.5.

$$Q = M_t V_0 \left(\sum_{j=1}^{k} n_j \theta_j \Delta H_j \right) \qquad (SI.3.5)$$

where V_0 is the initial volume of the sample cell [47]. To determine n, ΔH, and K from SI.3.5 a itteration of equation SI.3.6 can be made after peak intergration of the measured thermograph will give the heat evolvement as a function of molar ration [48].

$$Q = \frac{n[M]_t \Delta H V_0}{2} \left[1 + \frac{[L]_t}{n[M]_t} + \frac{1}{nK_a[M]_t} - \sqrt{\left(1 + \frac{[L]_t}{n[M]_t} + \frac{1}{nK_a[M]_t} \right)^2 - \frac{4[L]_t}{n[M]_t}} \right] \qquad (SI.3.6)$$

S.4 Emission lifetime of ACA

The decay of ACA was measured through a TCSPC measurement. with excitation with a 377 nm diode, 2048 channels and 10 000 as stop condition. The decay trace can be seen in Figure S.3, the lifetime was calculated to be 11.8 ns

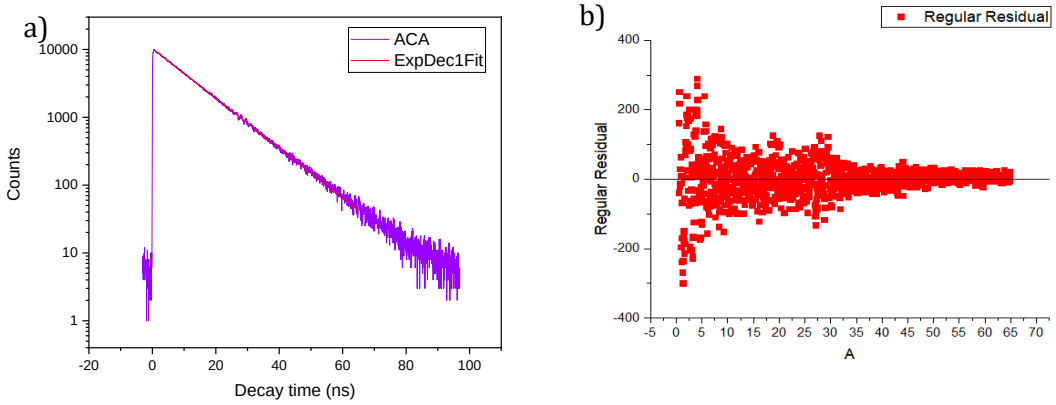

Figure S.3 *TCSPC measurement for ACA in DMSO. excitation 377 nm a) decay and mono-exponential fitting according to Equation 1b) regular residual from fitting.*

S.5 Emission lifetime of PCA

The decay of PCA was measuerd throgh a TCSPC measurment, with excitation with a 560 nm diode, and 2048 chaneles, measuerd at 673 nm. The decay trace can be seen in **Error! Reference source not found.**a. The decay was fitted to a mono-exponential decay, according to Equation 10.

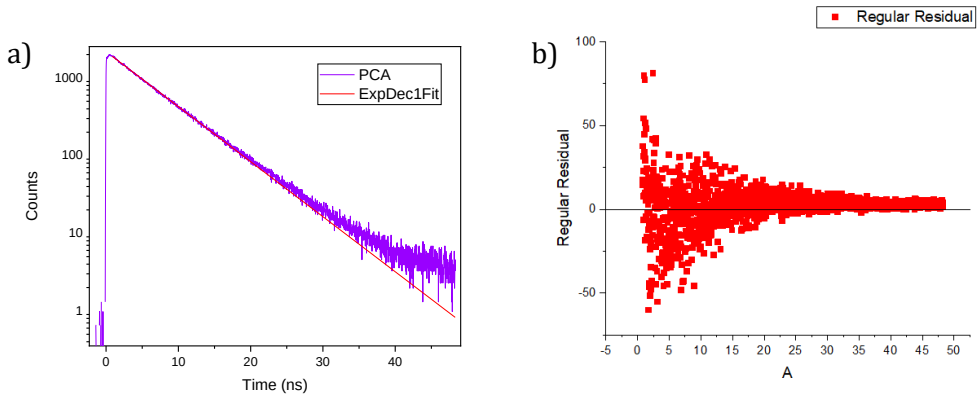

Figure S.4 *TCSPC measurement for PCA in DMSO, excitation 560 nm measured at 673 nm, a) decay trace, b) residual from mono-exponential fitting*

The lifetime was calculated to be 6.2 ns, the residual is presented in in **Error! Reference source not found.**b. **Error! Reference source not found.**

S.6 Titration of TBAOH to ACA

The effect in absorption and steady-state emission during titratation of 0.001 M TBAOH to ACA in DMSO can be observed in Figure S.5. A redshift in the absorption spectrum can be seen, with a decrease in intensity followed by an increase. In the emission spectrum a decrease in intensity and blueshift can be observed.

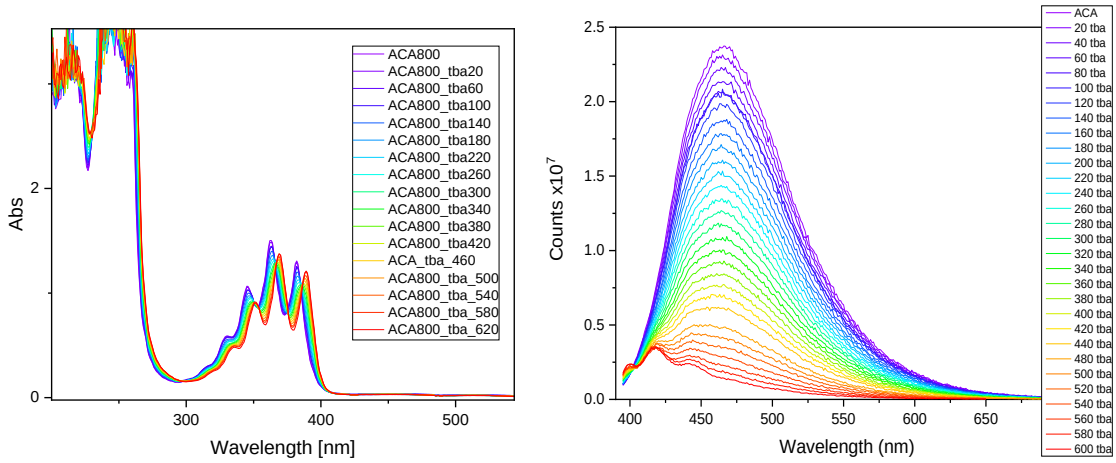

Figure S.5 *Titration of TBA to ACA in DMSO, from left to right absorption spectra, emission spectra with excitation wavelength 377 nm, slits 1 nm*

S.7 Titration of TBAOH to PCA

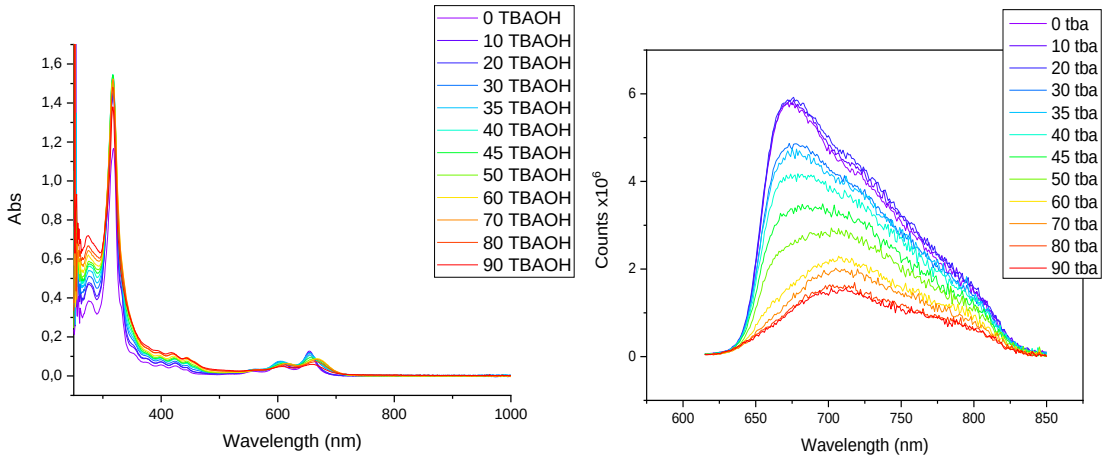

Figure S.6 *Titration of TBA to PCA in DMSO, from left to right absorption spectra, emission spectra with excitation wavelength 600 nm, slits 3 nm.*

The effect in absorption and steady-state emission of titratation of 0.001 M TBAOH to PCA in DMSO can be observed in Figure S.6. A redshift in the absorption at the S_1 band can be seen, with a decrease in intensity. The absorption at the S_2 band is increased, as well as the peak below 300 nm. In the emission spectrum a decrease in intensity and redshift can be observed.

S.8 Titration of sulphate salts to ACA

The effect on photochemistry of ACA when cations were presented was investigated by fully deprotonate ACA with DBU and then add sulphate salts solutions in DMSO in steps. The steady-

state absorption, emission, and TCSPC measurements were performed between each addition. The results from the two formers will herein be presented.

$ZnSO_4$ was added to ACA and DBU, the absorption and emission can be seen in Figure S.7. Absorption peaks before additions at 326, 341, 358, 376, 397 nm, after saturation 320, 334, 350, 369, 389, (363, 384) nm. Emission peaks before additions was observed at 409, 427, 455 nm, after additions at 397, 416, 440 nm.

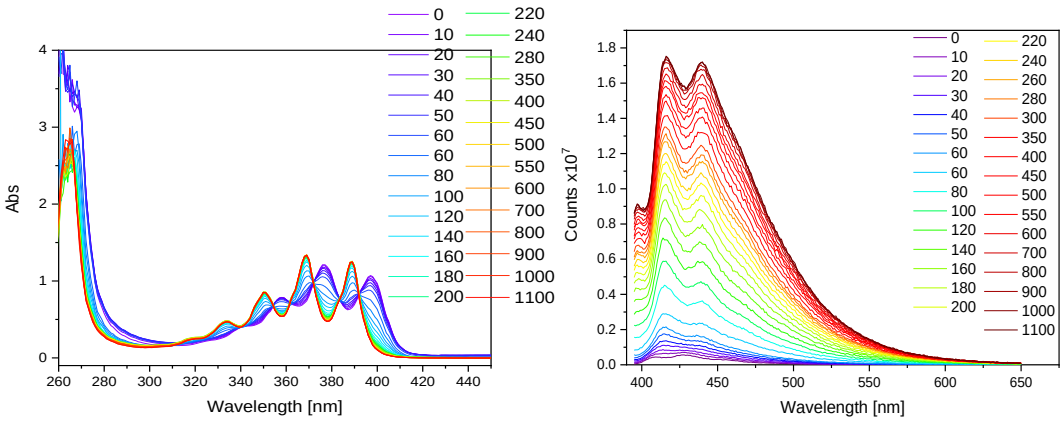

Figure S.7 *Titration of $ZnSO_4$ to ACA deprotonated with DBU in DMSO. From left to right, absorption, and emission spectrum*

$Al_2(SO_4)_3$ was added to ACA and DBU, the absorption and emission can be seen in Figure S.8. Peaks in absorption before additions were seen at 322, 339, 357, 375, 395 nm, after 315, 330, 347, 366, 384 nm. Emission peaks at 407, 427, 452 nm before addition and at 461 nm after.

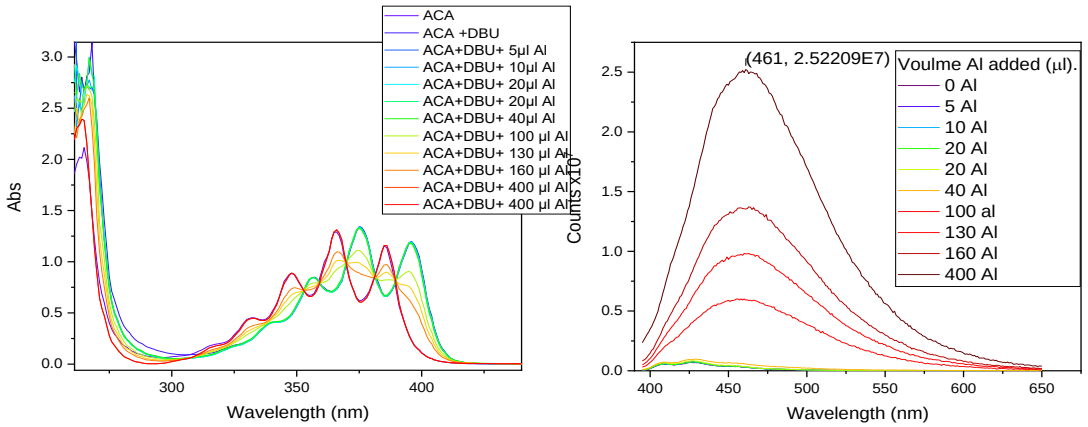

Figure S.8 *Titration of $Al_2(SO_4)_3$ to ACA deprotonated with DBU in DMSO. From left to right, absorption, and emission spectrum.*

Moreover, Na_2SO_4 was added to deprotonated ACA, see Figure S.9. No shifts could be detected, the absorption peaks at 409, 426, and 448 nm were constant throughout the titration. The same was for the emission peaks at (320, 339), 356, 375, 395 nm.

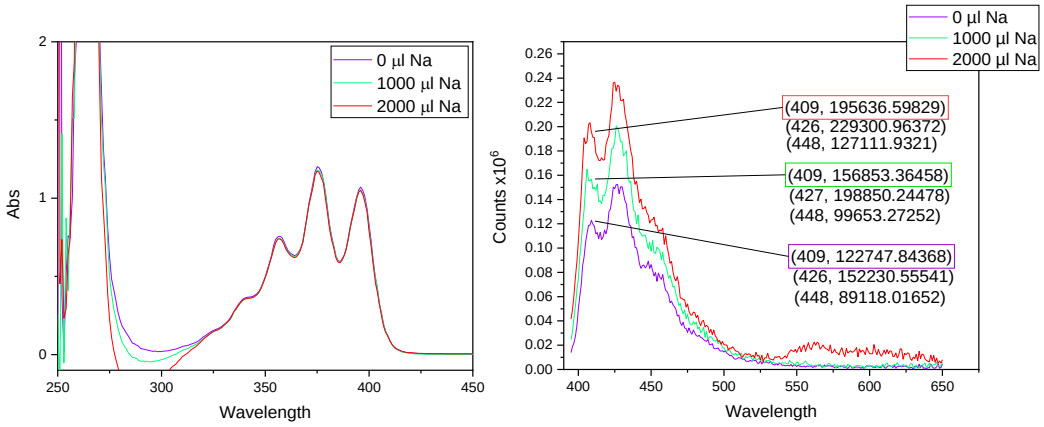

Figure S.9 *Titration of Na_2SO_4 to ACA deprotonated with DBU in DMSO. From left to right, absorption, and emission spectrum.*

To deprotonated ACA was $MgSO_4$ added, the absorption and emission spectrum can be observed in Figure S.10. At (323), 339, 356, 375, 395 nm were absorption peaks observed before any additions of salt solution. After peaks was seen at (334), 351, 369, and 388 nm. Emission peaks were shifted from 409, 430, 455 nm to 414, 438, and 467 nm.

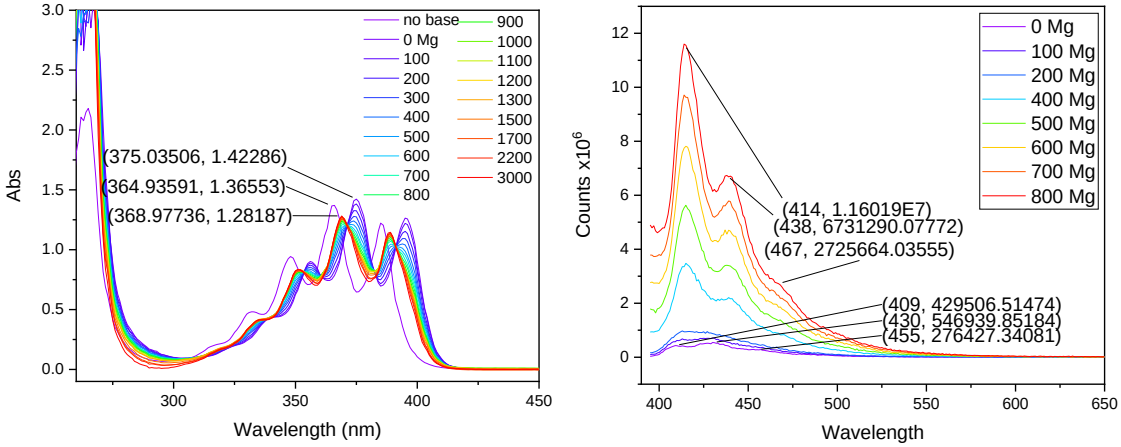

Figure S.10 *Titration of $MgSO_4$ to ACA deprotonated with DBU in DMSO. From left to right, absorption, and emission spectrum*

When $MnSO_4$ were added to ACA with DBU, no shifts in peaks could be observed, see Figure S.11.

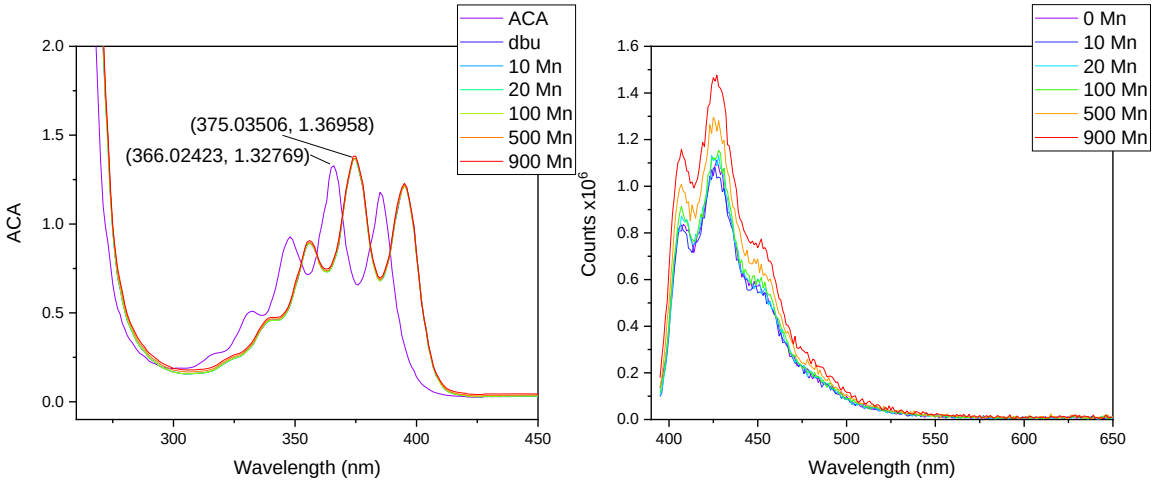

Figure S.11 *Titration of MnSO4 to ACA deprotonated with DBU in DMSO. From left to right, absorption, and emission spectrum.*

Lastly, $CaSO_4$ was added to ACA with DBU and no change in peaks could be observed, see Figure S.12.

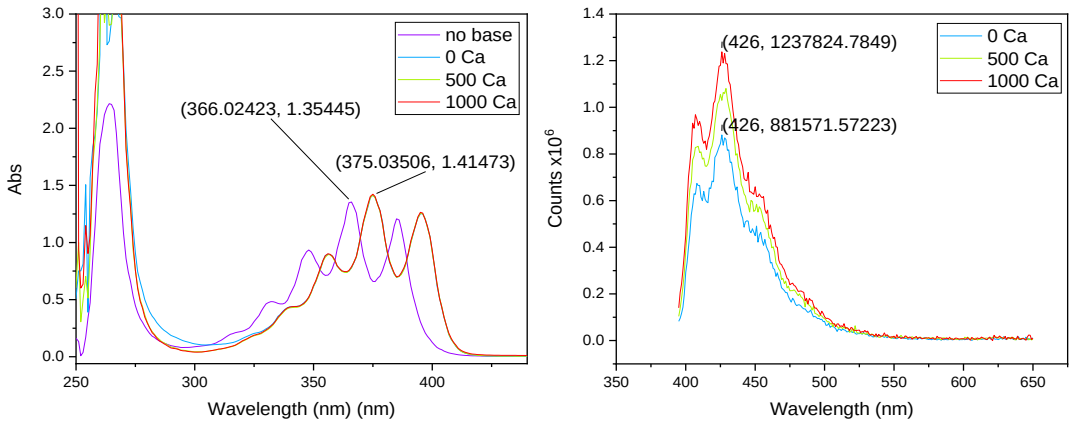

Figure S.12 *Titration of CaSO4 to ACA deprotonated with DBU in DMSO. From left to right, absorption, and emission spectrum*

S.9 Decay traces from TCSPC and TA

$ZnSO_4$ was added to three samples of ACA, one saturated with H_2SO_4, one where ACA been fully deprotonated with DBU and one with only ACA in DMSO. A TCSPC measurment was performed bwteen each addition of $ZnSO_4$ and the decay traces are preseneted in Figure S.13. The emission when acid was present is not changed upon addition of ZnSO4. When $ZnSO_4$ was added to only ACA a decrease in inclintion can be observed. Finaly, addition of $ZnSO_4$ to deprotonated ACA increase the emission lifetime. See Table 1 for derived emission lifetimes.

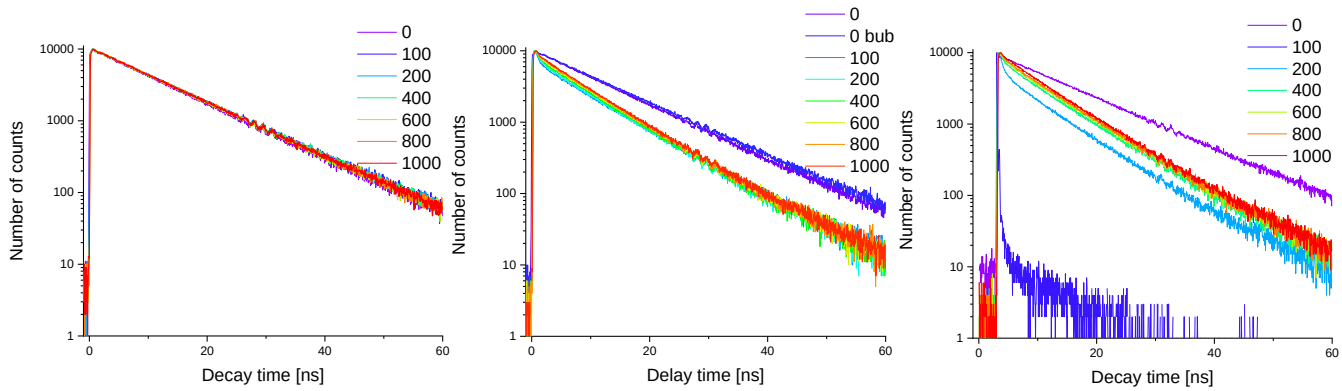

Figure S.13 *Emission lifetime measurements for titration of ZnSO4 to ACA. From left to right ACA+ H2SO4, ACA, ACA+ DBU*

The decay detected during TA measurements for ACA and ACA with Zn in excess in DMSO have been fitted to a monoexponential decay at four selected wavelengths. The obtained parameters from the fitting are presented in Table 1.

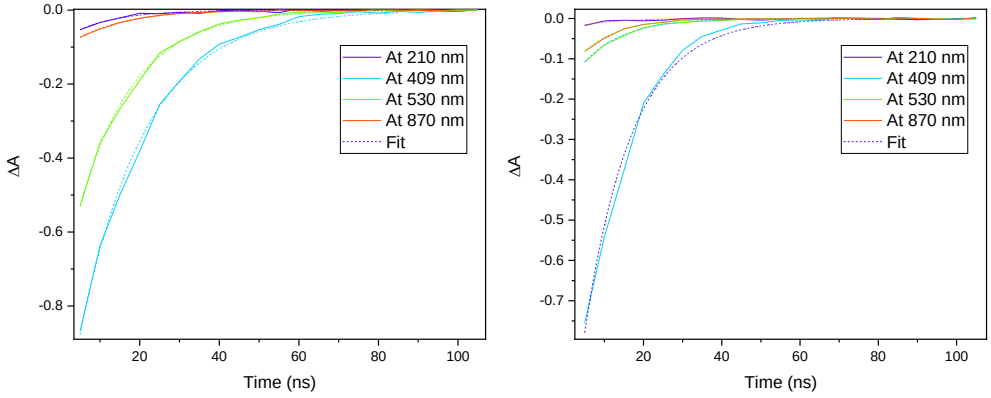

Figure S.14 *Decay at four selected wavelengths from TA measured with a CCD camera, to the left; ACA in DMSO, to the right: ACA with excess Zn in DMSO. The monoexponential fittings are included as dashed lines.*

In Figure S.15 two traces for similar samples of ACA in DMSO collected at two different days can be observed. The peak highs differentiate while the peak positions are the same for both samples, the concentrations were the same, 0.17 mM.

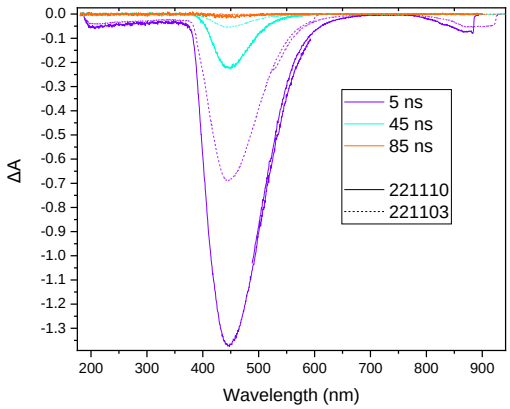

Figure S.15 *TA traces for two measurements of ACA in DMSO collected at 221110 and 221103, with 0.168 mM and 0.171 mM respectively. The dashed lines represent the latter.*

The decay traces for PCA obtained by TCSPC and TA are presented in Figure S.16.

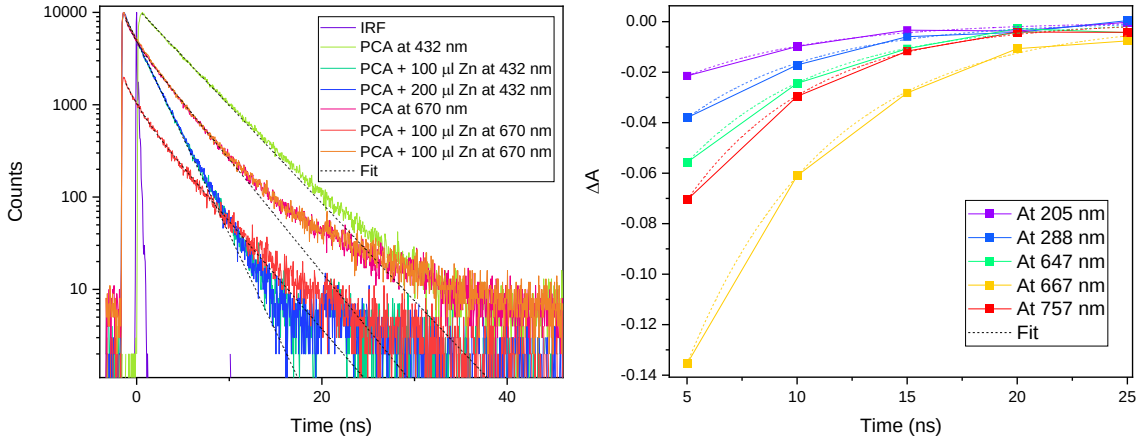

Figure S.16 *Decay traces for PCA in DMSO, to the left; TCSPC measurement, excitation wavelength 377 nm, detection wavelength 432 and 670 nm. To the right, TA measurements detected with the CCD camera. The fittings are included as dashed lines.*

DEPARTMENT OF CHEMISTRY AND
CHEMICAL ENGINEERING
CHALMERS UNIVERSITY OF TECHNOLOGY
Gothenburg, Sweden 2023
www.chalmers.se

CHALMERS
UNIVERSITY OF TECHNOLOGY